Investigating Kelvin wake deviations using multi-satellite remote sensing data

Master Thesis for Climate Physics

Ruben Scheffer

Supervised by:
Bas Altena (Daily supervisor)
Bert Wouters (First supervisor)
Erik van Sebille (Second supervisor)

Utrecht University

IMAU
August 6th 2020

Contents

1 Summary

In this work it is tried to gain geophysical oceanic information from the Kelvin wake angle, that is the angle of a wedge that contains the alignment of most waves that a ship produces through a movement differential with its surrounding. This angle, known as the Kelvin angle, has the special property that it seems to appear at a constant angle of 19.47°.

From optical satellite imagery displaying a ship wake this Kelvin angle caused by a ship can be observed and consequently determined. Measuring the Kelvin angle was done successfully, but is hindered by measurement errors, for which the standard deviation is used as a proxy. The mean standard deviation was determined to be 2.2°. This error can mainly be attributed to multiple user interpretations being possible when different Kelvin wakes are present in an image; the bow and stern of a ship as well as interference of the bow and stern wave can all produce a Kelvin wake. Also, each side of the ship can produce a Kelvin wake, sometimes leading to multiple Kelvin angles in a single image.

26 Kelvin angles are determined from repeated measurement, ranging from 13° to 21°, showing deviations from the normally constant Kelvin angle, but in accordance with recent literature showing deviations from 19.47°. By coupling the observed Kelvin angles to positional data (AIS) and environmental data a link between the Kelvin angle deviation and an external factor is sought for. Ship length, ship speed, water depth and a shear current do not show their theoretically predicted effect; which is likely caused by an oversimplified pressure distribution used in theory, due to which interference between bow and stern waves is ignored. It is likely that this interference causes the observed Kelvin angle deviations.

Furthermore the asymmetry of Kelvin wakes was investigated. Asymmetric wakes were found and were attempted to be linked to the surface current and wind. The hypothesised influence of their perpendicular components was however not observed; no clear relationship was found.

2 Introduction

In the late 19th century lord Kelvin already discovered a special property of ship waves [1]; the half-angle of the wave wedge is a constant 19.47°. This constant angle is not alone found in ship wakes, most objects travelling through water, even e.g. ducks, display this so-called Kelvin wake.

Only recently some deviations from this seemingly constant angle were found [2]-[4], which sparked interest in the Kelvin angle again. Some parameters found to cause Kelvin angle deviations are the ship speed[2][3], ship length[2], water depth[3] and shear currents[4]. So, the Kelvin angle seems to contain information about multiple nautical and oceanic parameters.

An advantage to retrieving such information stored in this Kelvin angle is that ships are spread out over the globe, thus Kelvin angles are also everywhere. If this Kelvin angle is observed, information on the environment of the ship may be extracted without disturbing the system by means of satellite remote sensing.

Recent literature is mostly focused on finding out what influences the Kelvin angle in a controlled environment, such as in a model [3][5][6] or in a laboratory [4]. This concept could however be inverted; if a Kelvin angle is observed, can it be used as a proxy for environmental information extraction? The aim of this study is exactly that: to gain knowledge about the ocean from Kelvin wakes observed in optical satellite imagery. This study takes an opportunistic approach; observed Kelvin wakes are coupled to several other sources of environmental information, where both the influence of parameters that do and do not have a theoretical indication to influence the Kelvin wake angle are explored. This is in contrast to literature, where often the influence of a single nautical or oceanographic parameter on the Kelvin angle is isolated.

The first reseach focus is answering the question: *'How can Kelvin angles be accurately measured from optical satellite imagery?'*. If reliably measuring the Kelvin angle is possible, the focus is laid on checking whether the theoretical relations, which are partially gained from models, apply for observations. This aims to then answer the main question asked in this research: *'What geophysical information can be gained from the Kelvin angle through optical satellite remote sensing?'*.

3 Background and Theory

3.1 Background

3.1.1 Optical remote sensing of ocean features

Optical satellite imagery can be used to observe a wide spectrum of ocean phenomena. Large scale phenomena can be observed using the MODIS sensor aboard the NASA Terra and Aqua satellites [8], which provides moderate resolution optical images (250 by 250 meters) alongside products in the non-visible light spectrum. The optical images have been used to detect: oil slicks [11][15][16], internal waves (which can have wavelengths of up to 10 kilometers [9])[10][17], stormwater plumes (water masses with decreased salinity compared to their surroundings) [18] and ocean water coloring [12][13][14].

To detect smaller phenomena higher resolution imaging is needed. For example Landsat 8, which can measure with a spatial resolution of up to 30 meters. Using Landsat 8 bathymetry can be mapped [22][21], coral reefs can be mapped [20] and the breaking of wind waves (typical wavelength in the order of 50 meters) can be investigated [19]. Also coastal shipping can be monitored [23].

Sentinel-2 provides optical data of a higher resolution than Landsat 8, up to 10 meters. This higher resolution can be employed to measure ocean surface current [25], small river plumes flowing into the ocean [24]. Furthermore ships and their wakes can be detected and recognized [26][27][28].

Commercial satellites provide even higher resolution imagery than Sentinel-2. Cubesats owned by Planet can provide optical images of up to a 3 meter resolution. These have been used to investigate: bathymetry [30], algae [29] and ship detection [31].

The preceding applications are by no means an exhaustive list of all applications. It does, however, show the possibility of observing ships and their wakes using high resolution imagery.

3.1.2 Ship wakes

A ship moving in a straight line creates a pattern of wakes; the rotation of the screw disturbs the water and the movement of the hull displaces a large amount of water. This wave pattern does not consist of a single wave, but is a more complex collection of multiple wave types [45]. A schematic of the wave pattern is depicted in Figure 1.

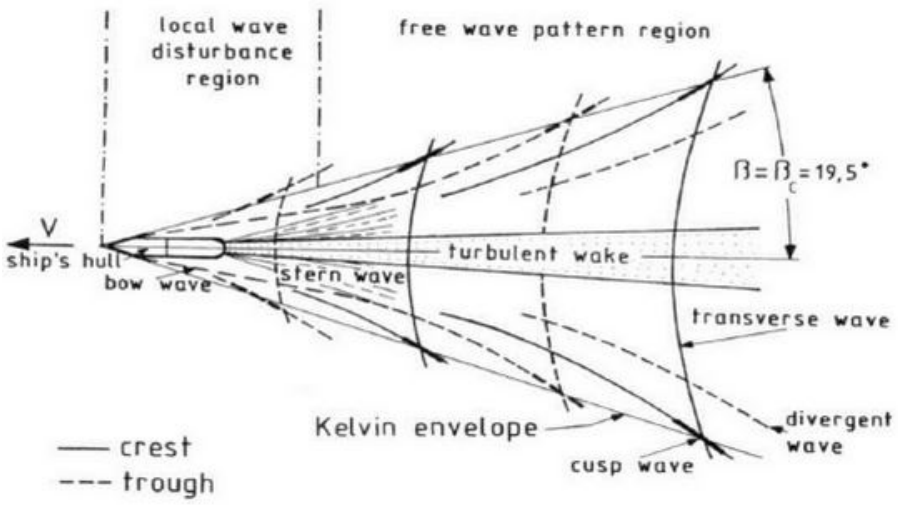

Figure 1: Schematic illustration displaying the observable ship wake pattern from a top-down view, from https://crisp.nus.edu.sg/ research/shipwakes/shipwakes.htm

The figure contains a collection of ship waves, which are:

- The turbulent wake, which is a wake directly behind the ship. The ship screws, as well as the hull create bubbles that alter the reflecting capabilities of the waves, creating a turbulent region close to the ship [56]. Further behind the ship a smooth region is seen. This wake has a limited width, not much wider than the ship that caused it. Bubbles shift the color of the ocean towards green, which allows it to be observed through its spectral properties [56].

- Divergent waves, which are waves that propagate oblique with respect to the ship heading. Their waveheight is typically low, making these waves hard to spot in optical images [53].

- Transverse waves, which are waves that are perpendicular to the ship heading and move parallel to the ship heading at initiation. Their waveheight is typically higher than that of the divergent wave, therefore it is spotted more easily in optical images, but not as often as the turbulent wake [53].

- Cusp waves, which are waves formed as a superposition of divergent and transverse waves [7]. The cusp waves form a V-shaped wake, which is also called the Kelvin wedge. The Kelvin wedge does always have a 19.47° angle with respect to the ship heading according to classical theory when a point source is assumed[1]. This angle of 19.47° can be derived mathematically,

which is displayed in appendix A. The total angle of the Kelvin wedge is $2\beta = 38.94°$.

The focus of this research is on the Kelvin wake angle. The theory subsection goes deeper into the Kelvin wake; it discusses Kelvin wake visibility in optical images and deviations of the Kelvin wake angle from the expected 19.47°.

3.1.3 Applications of Kelvin wake detection

The detection of the Kelvin wake can have multiple applications. Researching influences on the Kelvin angle [2][3][4][5][6], but also ship monitoring in the form of ship detection [26][50] and ship speed calculation on basis of the wake pattern [34]. Also military applications are found in the form of submarine detection on basis of the Kelvin wake [32][33].

3.2 Theory

3.2.1 Kelvin wake visibility

Kelvin wakes can be observed in optical satellite images [7][28][2]. The Kelvin wake can also be observed using synthetic aperture radar (SAR) [35][36][37][38][39]. An advantage of SAR is that imaging is not hindered by cloud cover or sun light[40]. In contrast optical satellite imagery is restricted by both cloud cover and a need for light; optical imagery passively observed reflected light, while SAR sends out relatively longer wavelength light that is consequently collected [35]. Also, combinations of both optical and SAR imagery are used for ship wake detection [40].

This research focuses on optical imagery as the available pixel resolution of freely available SAR data is limited (e.g. Sentinel 1 at 20 meters [41]). Optical images freely available from Sentinel-2 (10 meter resolution) [42] and images from Planet (3 meter resolution) [54] are investigated. The Planet imagery is available on a commercial basis, but free use is granted for research purposes.

The visibility of the Kelvin wake in optical satellite images was investigated in the study of Liu et al. (2018) [7]. This study found that the empiric probability of occurrence of Kelvin wakes in optical satellite imagery of a 2 meter resolution is small (27%) for cargo ships [7].

The relatively low empiric probability found by Liu et al. is due to a dependence on specular reflection; a process where incoming sunlight with elevation angle η_i is reflected by a surface and the elevation angle of the reflected light η_r equals η_i. This 'perfect' specular reflection is only observed for very calm water [43]. If water is not perfectly still less than 100% of the incoming light is reflected at the same angle of incidence, some of it is reflected at angles close

to η_r, which is called glossy or near-specular reflectance. As ship wakes are by definition disturbances of the water surface no 'perfect' specular reflection is expected; some light is reflected at an angle close to, but different from, the elevation angle of light reflected by specular reflection η_r.

The azimuth angle (angle with respect to the North in the surface plane) of reflected sunlight κ_r depends on the azimuth angle of incident sunlight κ_i. In 'perfect' specular reflection a ray of light continues in the same direction if seen from top-down, which means the azimuth angles are related by:

$$\|\kappa_r - \kappa_i\| = 180^\circ. \tag{1}$$

Again glossy reflection plays a role for disturbed water, the azimuth angle of reflected sunlight κ_r is then not strictly 180° larger than the incident angle κ_i, but close:

$$\|\kappa_r - \kappa_i\| \approx 180^\circ. \tag{2}$$

The process of specular and glossy reflection is illustrated in Figure 2.

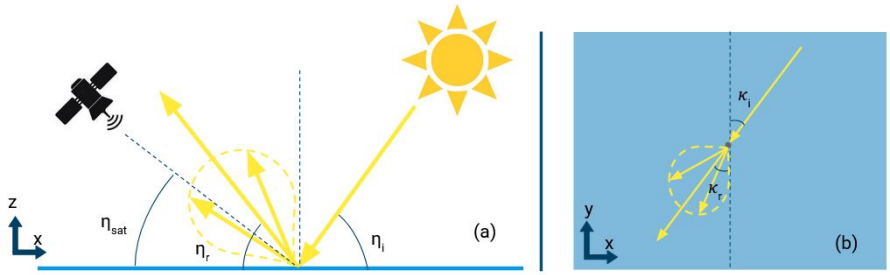

Figure 2: (a): Schematic view of sunlight coming in under a elevation angle η_i reflected by non-still water. Glossy reflection causes the light to be reflected at a elevation angle close to and centered around the angle of specular reflection η_r, which equals the incident elevation angle of the sunlight η_i. The water surface that reflects the light can be observed optimally if an observing satellite has an elevation angle η_{sat} equal or close to η_r. (b): A schematic top-down view of sunlight coming in under an azimuth angle κ_i reflected by non-still water. Glossy reflection causes the light to be reflected at an azimuth angle close to and centered around the angle of specular reflection κ_r (note that κ_r - 180° is actually displayed in the Figure). The water surface that reflects the light can be observed optimally if an observing satellite has an azimuth angle κ_{sat} equal or close to κ_r, which can also be defined as the requirement $\|\kappa_{\text{sat}} - \kappa_i\| \approx 180^\circ$ based on equation 2.

The reflection of sunlight by water waves is called sun glitter. This sun glitter is used to observe the Kelvin wake in optical satellite imagery. The Kelvin

wakes are best observed for a high solar elevation angle η_i, as the radiance of the sun glitter is the highest then [44]. Hence, the ability to observe Kelvin wakes strongly depends on the imaging geometry with respect to the illumination source and wave orientation. Optimally $\eta_{\text{sat}} = \eta_i$ and $\kappa_{\text{sat}} = \kappa_i + 180°$.

Furthermore, some ship parameters play a role in the detection of Kelvin wakes from sun glitter[53]. An increased ship's draft or velocity increases the size and elevation of its Kelvin wakes, which increases its visibility.

Finally, environmental factors can play a role in wake detection [53]. Wind can influence the wave pattern due to changing the roughness of the sea surface, which causes a shift of specular-like reflection to more diffuse-like reflection. It was however found that this effect is limited for Kelvin wakes [53].

The other environmental factor that plays a role is the presence of background swell waves; large wavelength waves created by wind, but no longer directly influenced by it. The Kelvin angle is impacted little if the amplitude of the swell waves is smaller than that of the Kelvin wake. However, if the amplitude of the swell waves is larger, swell waves become the highest amplitude waves in an image, causing Kelvin wakes to be no longer observed [53].

3.2.2 Kelvin wake deviations

The theoretical Kelvin wake angle of 19.47° is based on classical linear theory [7]. This theoretical Kelvin angle is not always observed however [2] - [4].

First of all, the hull Froude number Fr_L can influence the Kelvin angle [2]. Fr_L depends on the ship hull length L, the ship velocity U and the gravitational constant g. Deviations in the Kelvin angle were found to be scale-independent, which is why the effect is dependant on a dimensionless number, the hull Froude number. The definition of the hull Froude number is:

$$\text{Fr}_L = \frac{U}{\sqrt{gL}} \tag{3}$$

It was found that ships that have a hull Froude number higher than a critical value $\text{Fr}_{L,\text{crit}} \approx 0.5$ show a lower than expected Kelvin angle [2]. For $\text{Fr}_L < 0.5$ no deviation from the theoretical value is predicted, but for $\text{Fr}_L > 0.5$, the Kelvin angle β scales as:

$$\beta = \arctan\Big(\frac{\sqrt{2\pi\text{Fr}_L^2 - 1}}{4\pi\text{Fr}_L^2 - 1}\Big) \tag{4}$$

The scaling of Equation 4 is visualised in Figure 3.

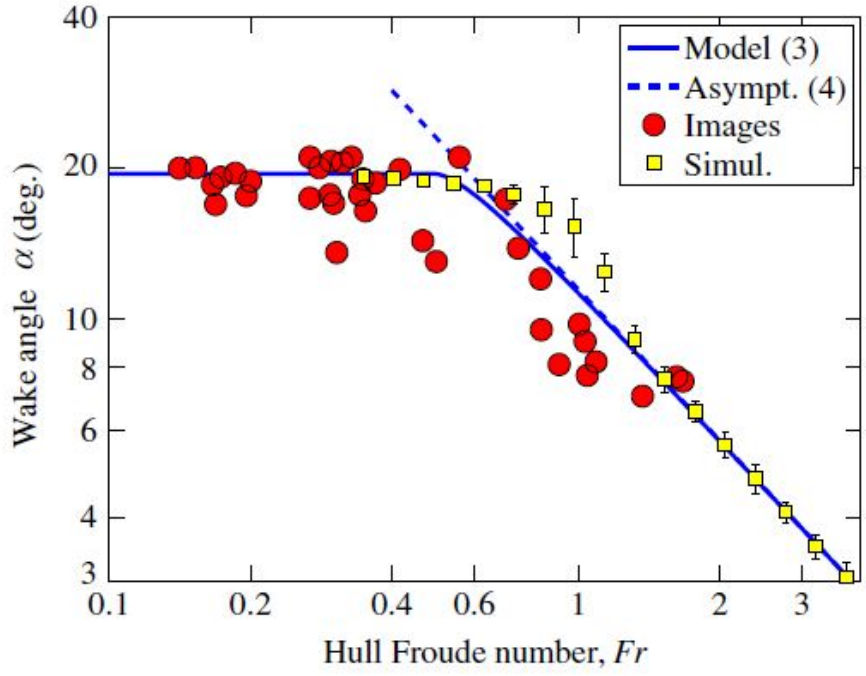

Figure 3: Log-log plot of the Kelvin wake angle α (named β in this thesis) as a function of the hull Froude number Fr_L from Rabaud et al. (2013). Red circles: angles measured from 37 airborne images. The measurement uncertainty is 1°. Blue line: model. Blue dotted line: asymptotic law. Yellow squares: numerical simulations. [2]

In Figure 3 the blue line shows a constant Kelvin angle for low hull Froude numbers (< 0.5) and a decrease for high hull Froude numbers (> 0.5) that scales as Fr_L^{-1}.

So, the observations of Rabaud et al. (2013) seem to contradict Kelvin's finding that the Kelvin angle is constant. However, in a theoretical study it was found that the deviations do not necessarily point to a contradiction; the wedge angle can always be constant, however the maximum cusp wave amplitude does scale as Fr_L^{-1} [51]. As a result, the apparent Kelvin wake β_{app} is introduced. β_{app} is the angle between the ship heading and the line through the highest amplitude waves, which is better observed in imagery due to the high amplitude waves.

Secondly, in certain situations the Kelvin angle β is influenced by the depth Froude number Fr_H [3]. The depth Froude depends on the ship velocity U, water depth H and gravitational constant g as:

$$\mathrm{Fr}_H = \frac{U}{\sqrt{gH}} \tag{5}$$

In Pethiyagoda et al. again a difference is made between the Kelvin angle β, which is the angle of the wedge that contains all ship waves, and the apparent Kelvin angle β_{app}, which is the angle between the ship heading and the highest magnitude waves.

The depth Froude number divides flow into a subcritical area ($\mathrm{Fr}_H < 1$), where both transverse and divergent waves are present, and a supercritical area ($\mathrm{Fr}_H > 1$), which is dominated by divergent waves. In the subcritical area the Kelvin angle β increases from the theoretical value of 19.47° at $\mathrm{Fr}_H = 0$ (infinite depth) to 90° at $\mathrm{Fr}_H = \mathrm{Fr}_{H,\mathrm{crit}} = 1$. In the supercritical area β again scales with Fr_L^{-1} as seen before in equation 4.

In Pethiyagoda et al. the similarity of the Kelvin angle β and apparent Kelvin angle depend on the unitless depth ratio $\delta = \frac{L}{H}$. If the water is sufficiently deep (δ small) the apparent Kelvin angle differs strongly from the Kelvin angle; where β rises from the theoretical Kelvin angle at $\mathrm{Fr}_H = 0$ to 90° at $\mathrm{Fr}_{H,\mathrm{crit}} = 1$, the observed β_{app} does not vary with changing Fr_H; β_{app} equals the theoretical Kelvin angle until the hull Froude number increases over 0.5, as seen earlier in Rabaud et al. (2013) [2]. For shallow water ($\delta >> 1$) the apparent Kelvin angle β_{app} behaves more like the Kelvin angle β, which increases from the theoretical Kelvin angle at $\mathrm{Fr}_H = 0$ to 90° at $\mathrm{Fr}_{H,\mathrm{crit}} = 1$ and then scales with Fr_H^{-1} above $\mathrm{Fr}_{H,\mathrm{crit}}$. The behaviour of β_{app} is not a 1 on 1 copy of β, but the difference between the two decreases for increasing δ. The difference between deep and shallow water is displayed in Figure 4, note that there still is a difference between β_{app} and β in shallow water.

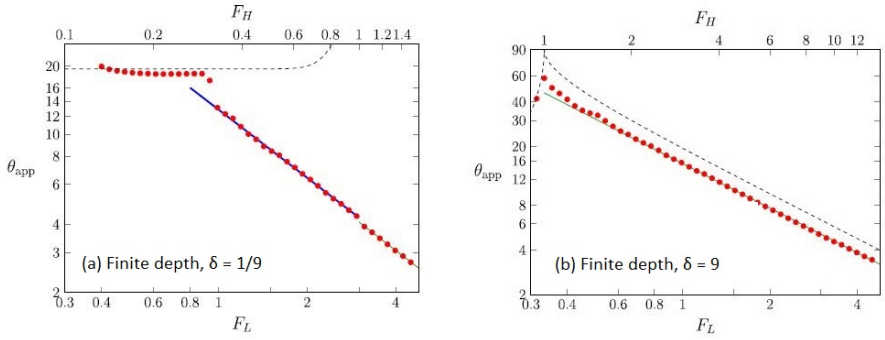

Figure 4: Measured apparent Kelvin wake angles θ_{app} (denoted by β in this work) plotted against the depth Froude number Fr_H and hull Froude number Fr_L on a log-log scale as red dots for a length/depth ratio of $\delta = \frac{1}{9}$, which is deep water (a) and $\delta = 9$, which is shallow water (b). The Kelvin angle β is displayed as a dotted line. The blue and green lines are theoretical asymptotes. Adapted from Pethiyagoda et al. (2015) [3]

.

Thirdly, a shear flow of uniform vorticity can also influence the Kelvin angle [4]. This influence depends on the strength of the vorticity and its direction with respect to the ship's heading. A side-on shear can lead to a larger Kelvin angle at the far side of the ship, leading to an asymmetric Kelvin wake. A head-on shear reduces the angle of both arms of the Kelvin wake. The mentioned study of Ellingsen (2014) is an experimental lab study; a model boat was moved through a water tank. This influences the water by the movement of the hull, but not by the rotation of a screw like for real ships.

Also, wind is expected to influence the Kelvin wake pattern [5]. Wind fields will lead to an asymmetry of the Kelvin wake and may cause a smaller windward Kelvin arm angle.

Finally, interference between the divergent waves created by the bow and stern of a ship can lead to different Kelvin angles [52]. It is found that the angle between the line along the highest amplitude waves and the ship heading (the apparent Kelvin wake β_{app}) is found to be different from the theoretical Kelvin wake for small hull Froude numbers ($\text{Fr}_L < \text{Fr}_{L,\text{crit}} = 0.59$). The apparent Kelvin angles are found to be in the range $13^\circ < \beta_{\text{app}} < 21^\circ$ and mostly located around the theoretical Kelvin angle.

4 Data and study region

4.1 Study region

The study is focused on a case study in the Strait of Singapore, which functions as a connection for cargo between the Strait of Malacca and the South China Sea. A map of the region is displayed in Figure 5.

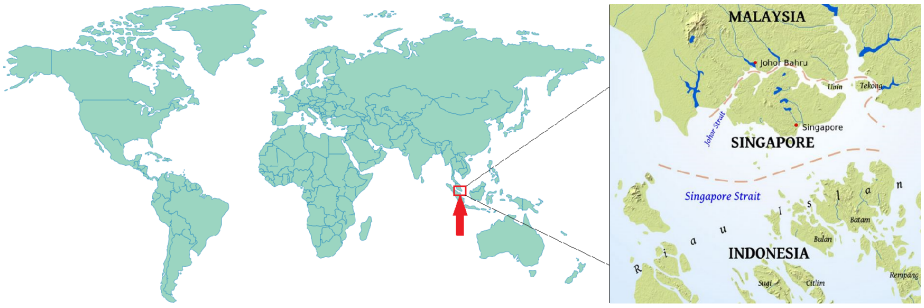

Figure 5: On the left a world map highlighting the Strait of Singapore, on the right a local map of the Strait of Singapore region.

A single region was focused on to make the amount of available data manageable. The exact spatial limits of the study area are:

- Latitude from 0.51° N to 1.58° N.
- Longitude from 103.11° E to 104.87° E.

The Singapore Strait was selected because of the following constraints:

- The strait of Singapore is part of a large shipping route, leading to a higher density of ships. This increases the ease of finding ships fit for this research.
- The Strait of Singapore is located at low latitudes, which means the sun is situated overhead for a considerable time of the year. This increases the intensity of sun glint, so it helps in observing the specular reflection of sunlight by the Kelvin wake.
- The shipping route through the strait of Singapore turns; ships travelling in different headings can be found. This increases the variety in the data.

The dependence on specular reflection limits the area to low latitudes. It does also determine the temporal limits of the study:

- Only observations in the late morning or early afternoon are used, as the sun is high overhead at these times. Also, the available satellites fly over the area in this time period only. Observing at a time were the sun is overhead improves the visibility of Kelvin wakes through specular reflection.

- Observations from April 9th 2020 until April 20th 2020 are used. There is no strong deviation in solar angles between the seasons near the equator, so this period was mainly chosen based on the lack of cloud cover at a first visual inspection of the data.

4.2 Planet Satellite Imagery

Kelvin wake observations are based on optical satellite images. Images are provided by Planet, a company offering commercially available satellite images at a high pixel resolution. However, using the freely available Sentinel-2 data set was also considered. Sentinel-2 was used to determine the surface current as described in section 5.2.4. However, the difference in resolution lead to the decision to focus on Planet imagery for the measurement of the Kelvin wake angle. The difference of resolution can be seen in Figure 6. The improved resolution can mainly be seen from the details of the ship and in the ship wake. The transverse waves are e.g. only visible in the Planet image.

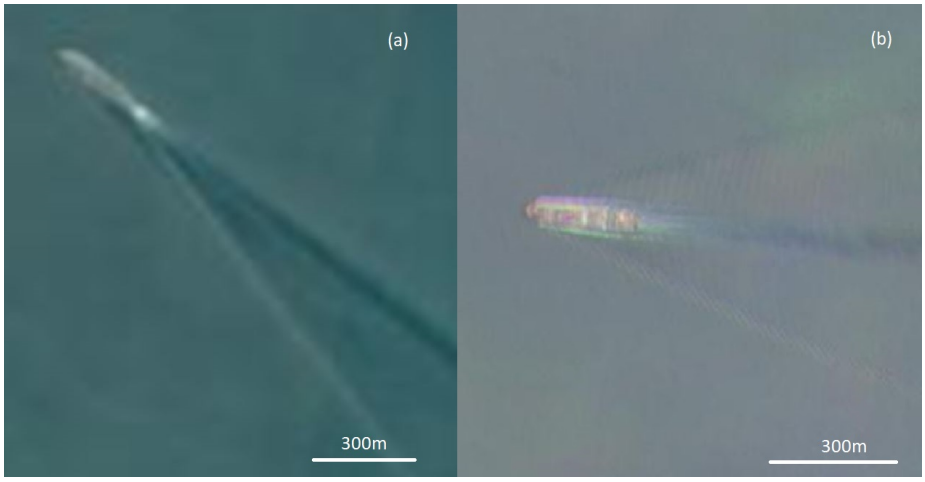

Figure 6: (a): 10 meter resolution Sentinel-2 image of a ship displaying a Kelvin wake located at 1.398°N, 103.194°E observed on 20-4-2020 at 11:37 Singapore time. (b): 3-meter resolution Planet image of a ship displaying a Kelvin wake located at 1.191°N, 103.606°E observed on 17-4-2020 at 11:35 Singapore time. A small time difference between the bands can cause the slight seperation of colors [46].

Different types of satellite imagery are offered by Planet, but only the 4-band PlanetScope constellation imagery is used. This constellation consists of approximately 120 cubesats (small satellites of 10 by 10 by 30 centimetres). The 4-band (R-G-B-NIR) PlanetScope Scene images have a pixel resolution of 3 by 3 meters. The four bands consist of blue (455-515nm), green (500-590nm), red (590-670nm) and near infrared (780-860nm) bands [54]. The cubesats typically cross the equator around 11:00AM local time. Each image spans a 24.6 by 16.4 km area and has a data size of approximately 100MB. A cutout of these images around a ship is used in this research to reduce the data size. A typical cutout used in this research has a data size of 1MB.

4.3 AIS Spire data

Similar to the Traffic alert and collision avoidance system (TCAS) for planes, Automatic Identification System (AIS) is a system that is used to avoid ship collisions [55]. The use of AIS is mandatory for almost all oceanworthy ships by 2021.

A transponder aboard a ship transmits different radio messages on regular intervals. Every two to ten seconds a location message, also known as dynamic message, is sent; this contains the MMSI (Maritime Mobile Service Identity, an unique ship identification number), position, time, course and speed of the ship. The location message does not contain information about the ship specifics

itself however. This data is transmitted every six minutes in a so-called static message. A static message contains among others the MMSI, ship type, cargo, length, draft and destination.

The radio data sent out omnidirectionally by ships is picked up by different receivers; ships, land stations and satellites. Other ships mainly use this data for collision avoidance, but land stations and satellites can collect these messages into a database, which may be used for other purposes.

Some of the other applications of such an AIS data base are found in literature. Besides collision detection the AIS is used for ship location monitoring [55][48], emission research[61][47] and making sea ice forecasts [49] amongst others[60].

Different companies provide AIS data, one of them is Spire [62]. Spire is a company that provides satellite data for a multitude of applications; data for maritime, weather, aviation and many more goals are available on a commercial basis. To gather the different types of data Spire builds an ever-growing network of cubesats (10x10x30 cm) which have sensors aboard that are specialised in collecting radio signals. These collect AIS data sent out by ships all over the globe, but also ADS-B plane signals and information on atmospheric temperature and pressure through GNSS-RO [62].

In this research an AIS data set provided by Spire is coupled to ships displaying a Kelvin wake in Planet imagery. A data set of over 1 million AIS messages (with a data size in the order of 1GB) gathered by land stations and satellites is used. This data consists of both dynamic and static AIS messages. Per ship this data set has a reduced coverage compared to the messages sent out every minute; a data point is available for a ship approximately every hour on average.

4.4 Auxiliary environmental data

Bathymetry data was gained from the most recent data grid of General Bathymetric Chart of the Oceans (GEBCO), which is the GEBCO_2021_Grid [63]. This product is based on hydrological surveys and has a resolution of 450 by 450 meters. The local bathymetry of the Strait of Singapore was downloaded, the data size of this bathymetry of this area is approximately 0.5MB.

Data on different variables is gained from ECMWF Reanalysis 5th Generation (ERA5), which models historical climate variables based on historical data. The sea surface temperature, surface current and 10-meter wind were all gained from ERA5 (data size less than 1MB). To be more precise, the data was gained from the 'ERA5 hourly data on single levels from 1979 to present' data set [64]. These modelled variables have a 31 by 31 kilometer spatial resolution and a temporal resolution of 1 hour. The ships observed in the Planet satellite imagery were observed over a time period of 12 days. The closest ERA5 data

points are coupled; for a temporal resolution of 1 hour the ERA5 data does never differ more than 30 minutes from the satellite observation time. While the variables gained from ERA5 show some temporal variation, the time difference is assumed to be small enough to neglect the difference.

Besides from ERA5, the surface current was also determined from swell wave movement in Sentinel-2 imagery. The surface current is measured by exploiting the changing sun glint between near-simultaneous overflight as described in Kääb et al. (2014) [65]. This results in observationally determined current data with relatively high resolution (640 by 640 meters). Two data points were removed from the observationally determined current, because they contained unrealistic values. These outliers were both approximately a factor 100 larger than the median current strength.

5 Methodology

5.1 Research Setup

The research goal is to investigate possible links between Kelvin angle deviations and environmental parameters. This Kelvin angle is determined from satellite imagery. If the Kelvin angle can be successfully linked to other parameters, a system could be designed to determine these parameters from a known Kelvin angle. This would allow for indirectly determining oceanic variables through remote sensing.

To find what links exist, in this research a data set is built up by combining an optical satellite image of a ship with both the ship information (gained from AIS) and environmental information. When a data set of ship satellite imagery and coupled locational information is built, they can be investigated to possibly find some relations between the Kelvin angle and environmental variables. This method and the extractability of the Kelvin angle are explored using a case study in the Singapore region.

5.2 Research implementation

The coupling of the imagery data, AIS and environmental data is displayed schematically in Figure 7.

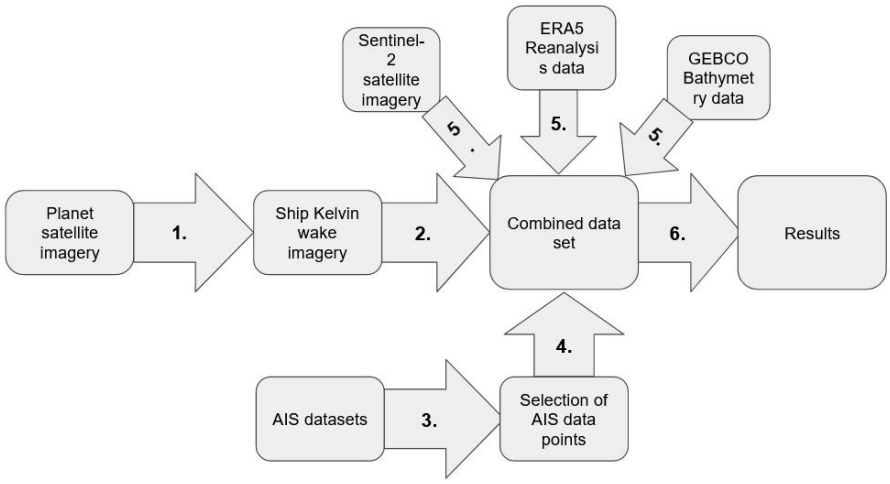

Figure 7: Diagram of data pathways, leading to combined data as a result. The arrows represent a processing step, where different numbers are different processing steps: 1: Image selection & processing. 2: Angle calculation. 3: Coupling of static and dynamic AIS data sets & filtering. 4: AIS-image coupling. 5: Auxiliary data coupling. 6: Data analysis.

Data processing steps 1-5 as described in the figure are explained in more detail in the following subsections. Step 6 is further explained in the results section.

5.2.1 Image selection and processing

The initial selection of images was made by manually looking through the available Planet satellite imagery archive, which is similar to what is done in earlier research [2]. Ships were sought for and where then selected if they display a Kelvin wake at one or both of its sides. As only the direct environment of the ship is needed, a cutout of the satellite image was made. The satellite images contained 12-bit data, which described 4 different bands (R-G-B-NIR) of which an average over the RGB-bands was taken. These RGB-bands are imaged at the same time, while the NIR band is acquired approximately 0.5 seconds later. So, the averaged bands have no time difference between them.

To subsequently ease the process of extracting the Kelvin angle from an image, image processing was performed if needed. If the wake pattern was hard to see, an Otsu threshold filter was applied, which has as goal to filter out the high intensity signal of the ship itself; this filter set the intensity of all pixels above a threshold value to zero. This threshold is automatically determined; a bimodal distribution is assumed and the threshold is set to separate these two distributions. In this research a bimodal distribution of pixel intensity does not always apply however; the ship is a high intensity signal and water a low intensity signal, but the intensity of the wake pattern is in between that of the ship and water. As a result, the wake is not always properly visible using the threshold set automatically. So, if the ship wakes were not visible the threshold value was set manually; it was assessed what the highest threshold value was that filters out the ship without filtering out the ship wake.

5.2.2 Angle calculation

From an image clearly displaying a Kelvin wake the Kelvin angle is measured. The angle was calculated by manually selecting four points; two points to determine the heading of the ship and two points to determine the heading of the Kelvin wake. A line is constructed in both cases, which give the heading of the ship γ_{ship} and heading of the Kelvin wake γ_{wake}. The Kelvin angle is consequently calculated as the difference between the ship heading and Kelvin wake heading:

$$\beta = \gamma_{\text{wake}} - \gamma_{\text{ship}} \tag{6}$$

This method is illustrated in Figure 8.

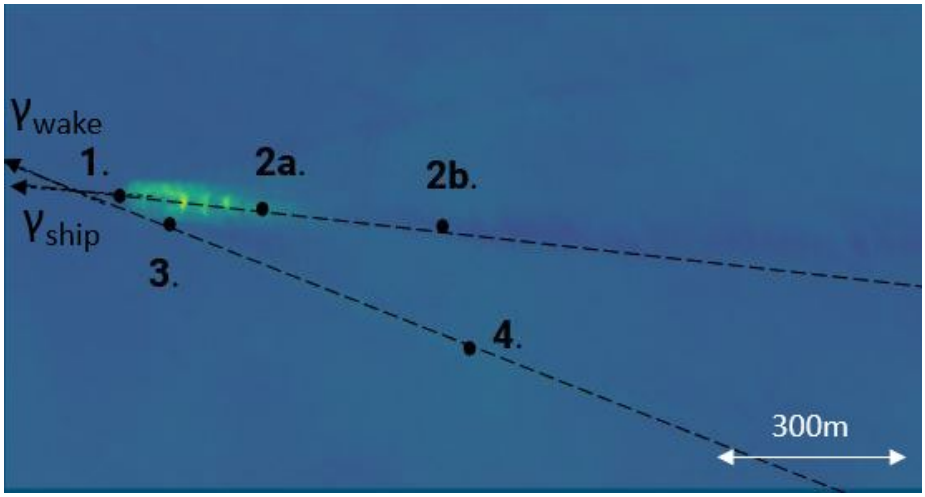

Figure 8: Overview of method to measure Kelvin angle. Point 1 is the bow of the ship, point 2a the stern of the ship, point 2b somewhere in the middle of the turbulent wake, point 3 is along the Kelvin wake close to the ship and point 4 along the Kelvin wake further away from the ship. Points 1 and either 2a or 2b were used to determine the ship direction γ_{ship}. Points 3 and 4 were used to determine the direction of the Kelvin wake γ_{wake}. Consequently, the Kelvin angle is calculated with equation 6.

Initially, point 2a (as seen in Figure 8) was used to calculate the Kelvin angle. This was later replaced by point 2b as more distance between the two points reduces the error, which is further explained in section 6.1.4.

5.2.3 AIS filtering and coupling to imagery

Automatic Identification System (AIS) data is coupled to ships to provide information about the ship, such as its velocity and draft. Two different types of AIS messages are received by the Spire satellites. These are static and dynamic messages. The static message contains a ship identification together with all non-changing information about the ship, such as its dimension and name. The dynamic message plays a role in collision-avoidance, as this message contains the ship position, course, heading and speed. The only common factor in both message types is the Maritime Mobile Service Identity (MMSI). Because both static and dynamic information are useful in the research, the data sets are coupled on basis of the MMSI.

After this combination, around 1 million AIS data points remain, produced by 500 different ships. A correct coupling has to be made to just 26 ship images. To ease this process, the AIS data set is filtered on basis of some criteria:

- Only large ships are included
- Only moving ships are included
- Only data points received in the late morning/ early afternoon are included

After this reduction in the amount of AIS points, the images are one by one coupled to a ship. This starts by further filtering the data for the specific ship; only the AIS data that is both close in time and position is needed. What remains is a data set that contains in the order of 100 points. Consequently, the remaining AIS points are compared with the position and time of the ship imagery. A direct comparison on basis of distance is not sufficient, because the ships are moving and there is often a time difference between the AIS data points and the time that an image was taken. As a way of comparing all data points at a same time, the AIS data points are interpolated to find their position at the time the satellite flew over t_{image}. Sophisticated ship path interpolation is performed in literature, e.g. in Kurekin et al. (2019) [55]. There a centripetal Catmull–Rom spline (CCRS) function is used to provide a smooth ship path based on multiple AIS data points.

Here we adopted a simpler interpolation method; linear interpolation. The linear interpolation is performed by calculating the time difference $\Delta t = t_{image} - t_{\text{AIS}}$ and assuming the speed and course remain constant for this time Δt. An interpolated position $\mathbf{X}^i_{\text{AIS}}$ of the AIS message is then found and can be directly compared with the position of the ship $\mathbf{X}_{\text{ship}}$. This process is illustrated in Figure 9.

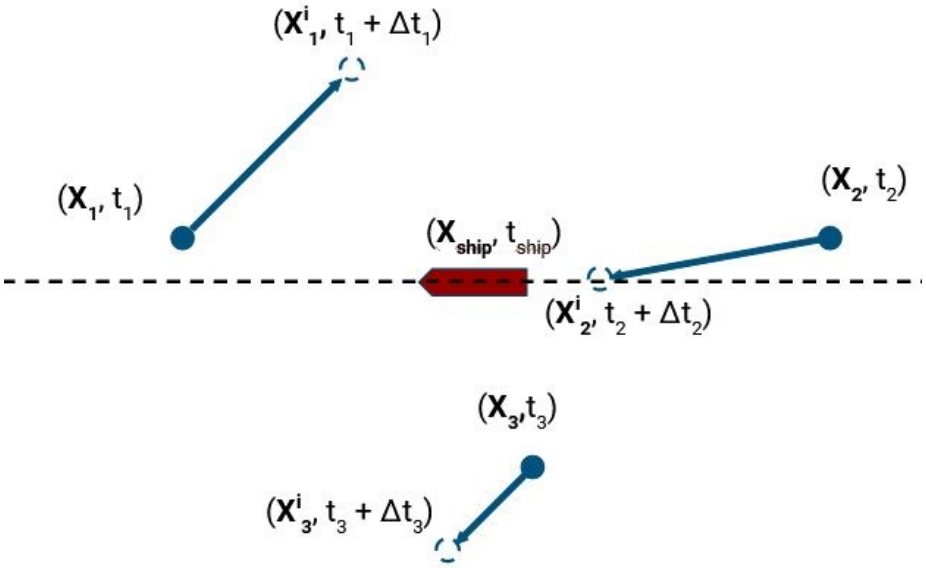

Figure 9: AIS - satellite imagery coupling process. A ship, displayed in red, is situated at position $\mathbf{X}_{\text{ship}}$ at time t_{ship}. Close by are three AIS data points, which are candidates to be coupled to the ship. These are shown as the solid blue points. To estimate their position at time t_{ship} linear interpolation is applied; the interpolation is shown as an arrow and the final result as a dotted blue circle.

Suitable AIS points are ranked by their interpolated distance to the ship at time t_{ship}. In case there are no AIS points within a reasonable distance of the ship ($< 1km$), no coupling is made. As a further test the heading of the data point and ship are compared. On basis of this comparison points are removed if the difference in heading is too large ($> 30°$). The closest remaining data point, if any, is then coupled to the ship. This method resulted in an AIS - imagery coupling in 11 of the 26 images.

5.2.4 Auxiliary data coupling

Coupling the auxiliary environmental data is more straightforward than coupling the dynamic data of the AIS. The data of the different environmental data sets is stored in grids. The time and position of imaged ships are known, so a ship can be coupled to a certain position and time in the environmental data. As the time difference between the satellite overflight and grid cell data is small (less than 30 minutes) compared to their temporal variability this time difference is neglected.

6 Results

The results consist of Kelvin angles observationally determined from 26 Planet satellite cutouts, which are gained from 18 different Planet image subsets. An analysis of the calculation of Kelvin angles from the observations and its errors is displayed first, followed by relating these found Kelvin angles to variables gained from the AIS Spire data (ship dimensions) and environmental data (bathymetry from GEBCO, sea surface temperature, wind and surface current from ERA5 and the surface current measured from Sentinel-2 images).

6.1 Kelvin wake angle measurement

Calculating the Kelvin wake angle based on observational data results in different types of errors; a measurement error introduced by the dependency on manual work, as well as a systematic error due to the method itself. These errors were investigated. Also, the expected Kelvin angles $\widetilde{\beta}$ are predicted on basis of theory.

6.1.1 Expected Kelvin angles

In section 3.2.2, different causes for a deviation in the Kelvin angle β are given. Firstly, the hull Froude number Fr_L (which is determined by equation 3) can lead to a decreased β if $\mathrm{Fr}_L > 0.5$ [2]. However, the hull Froude numbers of the analysed images are in the range $0.03 - 0.16$. In other words, the data set consists of large (200-330 meters) and relatively slow ships (7-16 knots). For this reason, no deviation of the Kelvin angle β is expected on basis of the hull Froude number.

Secondly, the Kelvin angle can also be altered depending on the depth Froude number Fr_H (which is determined by equation 5) [3]. The effect of the depth Froude number depends on the ratio of the ship length L and water depth H: $\delta = \frac{L}{H}$. For values of $\delta >> 1$ (shallow water) the water depth is expected to play a role. For the 11 of the 26 observed ships δ is calculated. It was calculated for only 11 of the 26 ships because the ship length L is gained from AIS Spire data, which was only successfully coupled 11 times. The values are displayed in Figure 10.

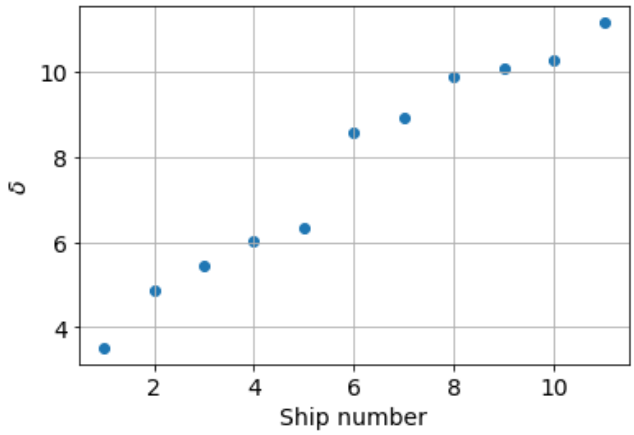

Figure 10: The ratio of ship length and water depth δ of 11 ships from the observational data. The ship number is an arbitrary, meaningless value, so the ships are displayed in ascending order of δ.

Although the ship length of 15 out of 26 observed ships is not known, they can be estimated to be 275 meters long (close to the average ship length in this observational data set) to give a rough estimate of the values of δ. As the water depth is in a similar range as the ships displayed in Figure 10 one can assume that $\delta >> 1$ for all 26 ships in the observed data.

On basis of the high values of δ it can be expected that the depth Froude number alters the observed Kelvin angle [3]. In what way the Kelvin angles are altered depends on the depth Froude numbers, which was calculated for 11 observed ships that were coupled to the AIS data. These values of the depth Froude number Fr_H are shown in Figure 11.

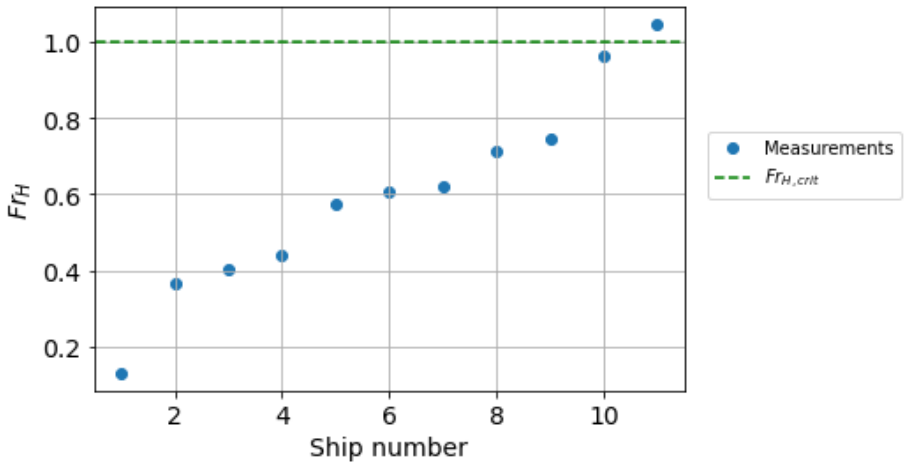

Figure 11: Depth Froude number Fr_H calculated for 11 ships from observational data in blue. The theoretical value $Fr_{H,\mathrm{crit}} = 1$ in green [3]. The ship number is an arbitrary value, so the ships are displayed in ascending order of Fr_H.

Based on the values of δ and the depth Froude numbers seen in Figures 10 and 11 and comparing them with Figure 4 it can first be seen that plot (b) of Figure 4 has a high value of δ in common with the observed data. So, based on Pethiyagoda et al. (2015) it can be expected that the Kelvin angle is larger than the theoretical value for all observed data. An exact prediction of the Kelvin angles can not be made; the behaviour of the observed apparent Kelvin angle β_{app} depends on the ratio of ship length and water depth δ. This dependency is displayed in Figure 4, but only known for certain values of δ. This figure is produced by Pethiyogada et al. (2015) from simulations, no mathematical relation is given to calculate the expected Kelvin angles for different values of δ. A general expectation of the angles can be made, which is a positive deviation of the Kelvin angle, in particular for Fr_H close to $Fr_{H,\mathrm{crit}} = 1$, where it is expected to approach 90°, but also to a lesser degree for the other data points.

Also, a shear of constant vorticity can give rise to alterations of the Kelvin angle [4]. This alteration depends on the direction of the vorticity; one parallel to the ship could reduce or increase both arms of the Kelvin wake equally, while a perpendicular component is expected to cause an asymmetry in the wake pattern. The auxiliary data shows that a surface current is predicted (since it is modelled) in the measurements, and as a consequence an effect of the current on the angles may be found. Asymmetry may be be found in the images where the Kelvin wake is visible at both sides of a ship.

Furthermore wind could alter the Kelvin angle[5][6]. The windward Kelvin arm angle is expected to be reduced. Also an asymmetry in the wake pattern

may arise if the wind has a perpendicular component with respect to the ship heading.

Finally, interference between waves from the bow and stern of the ship may cause Kelvin angle deviations [52]. This theoretical relation was found after most of the results were found, the effect of interference is therefore further looked at in the discussion.

6.1.2 Kelvin angle calculation

The Kelvin angles were observationally determined from satellite imagery as explained in section 5.2.2. To investigate the consistency of this Kelvin angle determination, it was repeated five times for each ship. These results were used to determine a mean Kelvin angle $\bar{\beta}$ and a standard deviation σ. This standard deviation is defined as:

$$\sigma = \sqrt{\frac{1}{N}\sum_{i=1}^{n}(x_i - \bar{x})^2} \tag{7}$$

where N is the amount of measurements, x the measured variable and $\bar{x}$ the mean of this measured variable. The standard deviation is used as a measure for the measurement error.

The mean Kelvin angle and standard deviation are calculated for 26 ships in satellite imagery and is displayed in Figure 12. As the ship number is an arbitrary value, the measurements are sorted in ascending order on basis of the mean Kelvin angle.

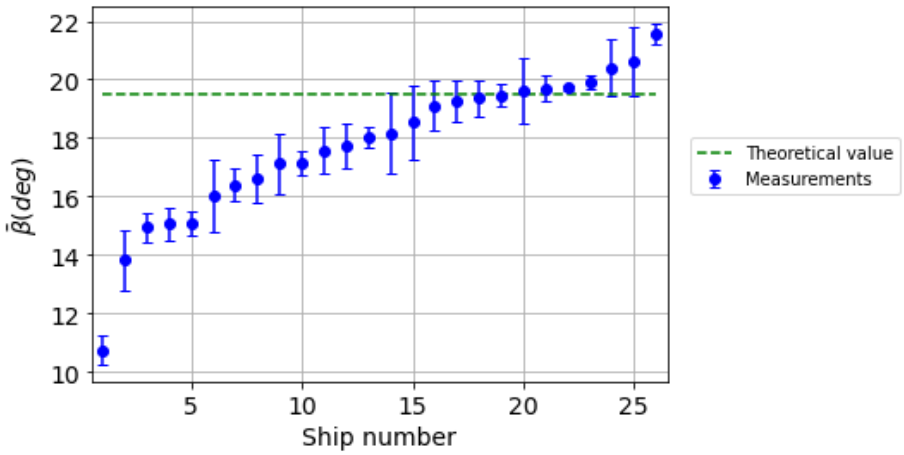

Figure 12: The mean Kelvin angle $\bar{\beta}$ and its standard deviation σ determined from repeated measurement of 26 ships in satellite images in the Strait of Singapore is displayed in blue. The theoretical value for the Kelvin angle of 19.47° is displayed as a dashed green line.

What can be seen in Figure 12 is that the Kelvin angles range from $11° - 22°$; a visible deviation from the theoretical value of 19.47 °. The values seem to be quite evenly spread between angles of $14° - 22°$ with a single outlier at 11°. The standard deviation ranges from 0.1° to 1.4° and is 0.7° on average. For 8 of the 26 measurements the mean Kelvin angle $\bar{\beta}$ is closer than one time its standard deviation to the theoretical Kelvin angle, which can be seen in the figure from the fact that the errorbar intersects with the dashed line for the theoretical value.

6.1.3 Measurement error

In section 6.1.2 a standard deviation was calculated on basis of repeated measurements. As the standard deviation σ is larger than zero this means that the measurements were not precisely replicated, but differed in repeated measurement; this is the cause of a measurement error. It is hypothesised that this measurement error is dependant on who measures the Kelvin angle; which would entail a measurement bias.

To research the existence of a measurement bias the Kelvin angle calculation (as described in section 5.2.2) was performed by three other persons. Two of them contributed a single run of determining the Kelvin angles, while one contributed a data set based on five repetitions of determining the Kelvin angle, similar to the one that was used to produce Figure 12. Figure 13 then shows the results of this investigation.

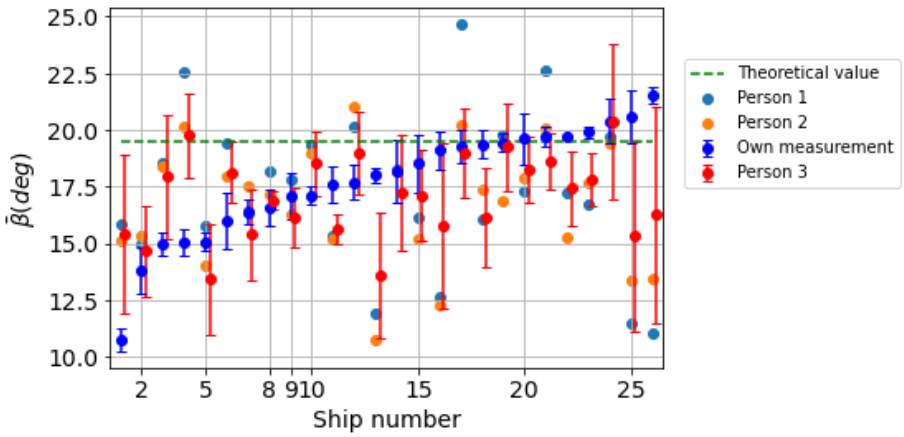

Figure 13: The mean Kelvin angle $\bar{\beta}$ and its standard deviation σ determined by the author are displayed in blue, similar measurements contributed by another person are displayed in red. Two other single contributions are displayed in grey and orange. The theoretical value for the Kelvin angle of 19.47° is displayed as a dashed green line.

As can be seen in Figure 13, there is no full agreement between own measurements and added external measurement. On one hand, measurements do agree for some some ships, e.g. at ship numbers 2, 8 and 9 in Figure 13. The mean Kelvin angles differ little ($\sim 1°$) at these points. On the other hand, there are multiple cases where very different results were found depending on who performed the angle calculation, e.g. ship numbers 25 and 26. The difference in angles found can be as large as (10°) there.

As the external contributions in a lot of cases do differ from the results found earlier, the hypothesis that measurement bias plays an important role in determining the Kelvin angle can be confirmed. The measurement bias may be caused by different options for a Kelvin being present. In some cases both the bow and stern of a ship produce a Kelvin wake, which can slightly differ in angle. Multiple options for the Kelvin angle are also found if the Kelvin wake is visible at both sides. Also, even a single arm of the Kelvin arm is susceptible to some degree of interpretation.

Due to the role of the measurement bias the initial results in Figure 12 do not fully cover all options for the Kelvin angle. It is shown that relatively precise measurements can be made, however the accuracy of these measurements is lacking, as often multiple Kelvin angles can be found (bow/stern or left/right).

A combination of all the contributions is used to generate a new mean Kelvin angle and standard deviation. The new results, including the external contributions, can be seen in Figure 14. As the order of the measurements is non-important, the results are again sorted on ascending mean Kelvin angle $\bar{\beta}$.

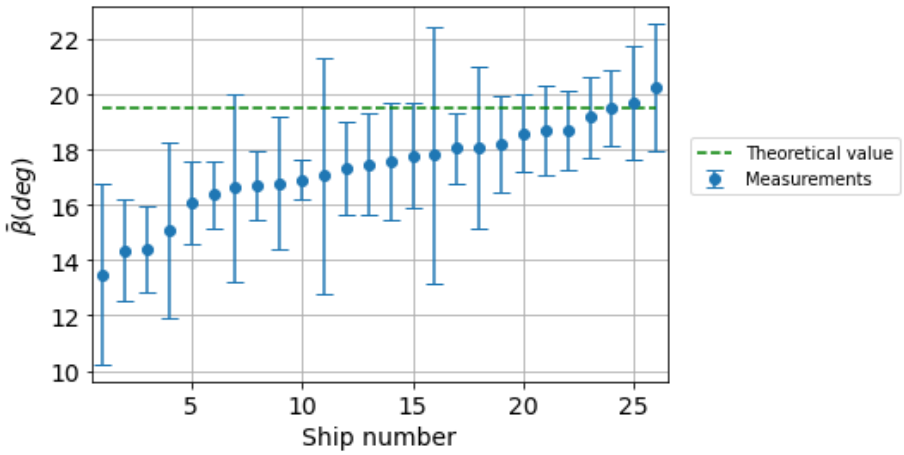

Figure 14: The mean Kelvin angle $\bar{\beta}$ and its standard deviation σ of 26 images determined using 12 contributions per image, where the 12 contributions are from 4 different persons. The theoretical value for the Kelvin angle of 19.47° is displayed as a dashed green line.

By comparing Figure 14 to Figure 12 it can be seen that the average angles range from 13° to 20 °, which is a smaller spread than the 11° to 22 ° that was found before. Furthermore, the errorbars are larger, as the mean standard deviation $\bar{\sigma}$ has increased from 0.7° to 2.2°. As a result, now 14 of the 26 Kelvin angle measurements errorbars intersect with the line depicting the theoretical Kelvin value; in 14 of the 26 Kelvin angle measurements lays the mean Kelvin angle $\bar{\beta}$ less than one time its standard deviation from 19.47°.

6.1.4 Systematic error

The standard deviation shown in Figures 12-14 is introduced through inconsistency in the four points chosen to determine the Kelvin angle.

The method itself may also introduce an error, a systematic error. This systematic error is estimated as follows: a satellite image has square pixels of pixel resolution x by x meters. Assume a ship of length L (it is assumed that x fits n times in L with n an integer) that is heading North, which equals a ship heading γ_{ship} of 0°. The bow and stern of the ship are placed in the middle of the pixels; moving the bow to the right to the edge of the pixel (a movement of $0.5x$ meters) results in the bow still being located in the same pixel, while a small movement and thus rotation has happened. Assume a similar translation of the stern in the opposite direction as the bow. If the ship heading γ_{ship} is determined using two pixels as section 5.2.2 explains, then it remains 0°. However, in reality the new heading is now $\arctan(\frac{x}{L})$, due to the bow and stern

being moved. This is an error introduced due to a certain pixel resolution x. More generally the two selected pixels are not necessarily the bow and stern, but can be any two pixels. The error in the heading e_{head} for any two pixels with sides x and distance between the pixels l is then (according to this estimation):

$$e_{\text{head}} = \arctan(\frac{x}{l}) \tag{8}$$

The Kelvin angle determination relies on the difference between two angles, the ship heading and Kelvin wake heading. Both are susceptible to the systematic error; assuming similar pixel distances l the total error can using error propagation ($e_{\text{total}} = \sqrt{e_1^2 + e_2^2}$) be determined to be:

$$e_{\text{sys}} = \sqrt{2}\arctan(\frac{x}{l}). \tag{9}$$

Equation 9 demonstrates why it is preferable to use the turbulent wake and not the ship stern to determine the heading of a ship. A larger distance between the measurement points l decreases the error. The systematic error is then estimated for the used Planet satellite imagery, which has a pixel resolution x of 3 meters and an estimated pixel distance l of 750 meters. Using equation 9 the systematic error is 0.32°, which is smaller than the measurement error of 2.17°.

6.2 Relation to environmental variables

A link between the calculated mean Kelvin angles as shown in Figure 14 and other variables is sought for. A wide range of variables was tried to link to the Kelvin angle; AIS Spire data in the form of ship length, width, draft and velocity as well as environmental data in the form of sea surface temperature (SST), water depth, current and wind. Some of these variables have theoretical indications that they may influence the Kelvin angle, but ones without theoretical indication are also looked at.

6.2.1 Mean Kelvin wake angle dependence on scalars

First, a relation between the mean Kelvin wake angle $\bar{\beta}$ and the ship length L (from AIS Spire data) is investigated. On basis of theory the ship length can influence the Kelvin wake by altering the hull Froude number Fr_L [2]. However, the values calculated for Fr_L are all too low to expect an altered Kelvin angle. So, no relation between the ship length and Kelvin angle is expected. The mean Kelvin angle as a function of the ship length L and as a function of the hull Froude number Fr_L can be seen in Figure 15. As the ship length L is gained from the AIS data, the amount of data points is reduced to 11; AIS can not always be coupled to a ship.

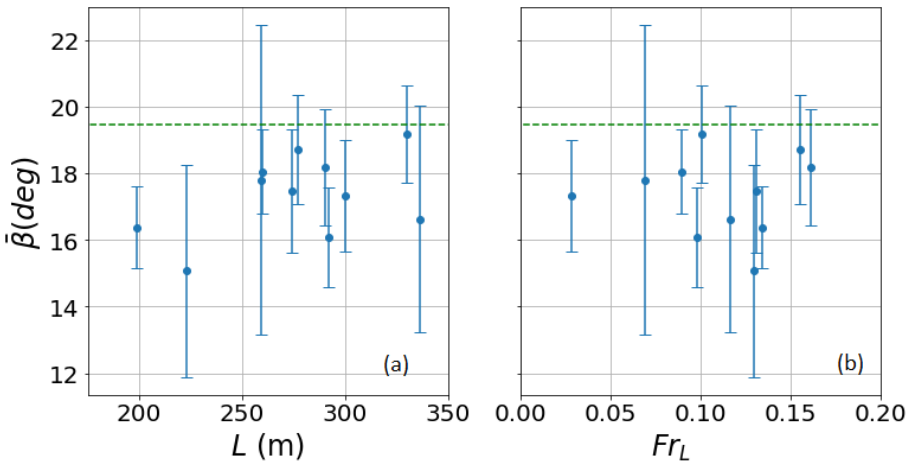

Figure 15: Mean Kelvin angle $\bar{\beta}$ as a function of the ship length L (a) and as a function of the hull Froude number Fr_L (b) based on 11 ship images is displayed in blue. The reduction in amount ofdata points is a result of the dependence on AIS data, which was only coupled successfully in 11 images. The theoretical value for the Kelvin angle of 19.47° is displayed as a dashed green line.

As seen in Figure 15(a) there is a spread in the ship lengths from 200 - 330 meters. All angles are smaller than 19.47°, which is not expected on basis of the hull Froude number, because the values of Fr_L are lower than 0.5 as seen in Figure 15(b). There is no clear reliance of the mean Kelvin angle on either the ship length or hull Froude number in this data. This agrees with the expectation, because theoretically the values of Fr_L are too low to influence the Kelvin angle.

The AIS Spire data set also contains ship width and ship draft data. These variables have a high correlation with the ship length. As a result the figures look very similar to Figure 15(a). Therefore, these are shown in Appendix B.

Furthermore, a relation between the mean Kelvin wake angle $\bar{\beta}$ and the sea surface temperature T, which is obtained from ERA5 data, is investigated. There is no theoretical indication that the Kelvin angle is influenced by the SST. So, it is not expected to find a relation between $\bar{\beta}$ and T. The mean Kelvin wake angle $\bar{\beta}$ is plotted against the sea surface temperature T in Figure 16.

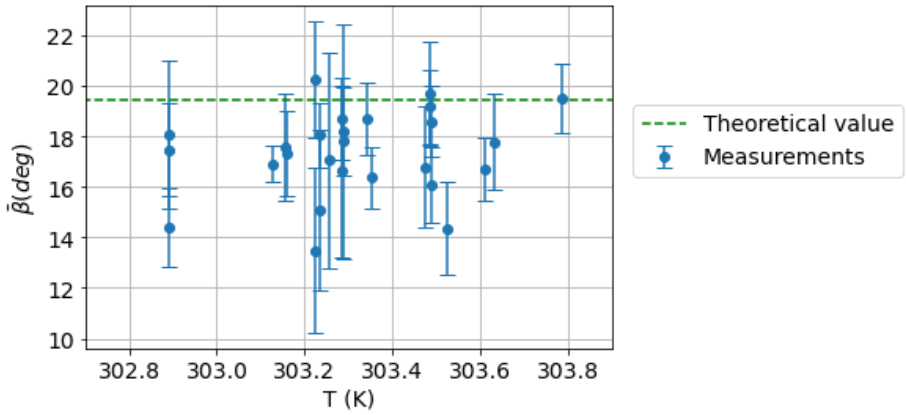

Figure 16: Mean Kelvin angle $\bar{\beta}$ as a function of the sea surface temperature T based on 26 ship image is displayed in blue. The theoretical value for the Kelvin angle of 19.47° is displayed as a dashed green line.

The spread in T is limited to 1 degree Kelvin. Also, the values of $\bar{\beta}$ show no clear positive or negative trend; this is strengthened by the observation that for a T of 303.2K multiple values of $\bar{\beta}$ are found, which range from as low as 14° to as high as 20°. All in all there is no relation found between the sea surface temperature T and mean Kelvin angle $\bar{\beta}$, which agrees with the expectation, as no theoretical link is known.

There is an indication that the Kelvin angle can be influenced by low water depths, as seen in theory; higher Kelvin angles can be found depending if the ship is in relatively shallow water (which is defined as a length/depth ratio $\delta >> 1$). The increase in Kelvin angle then depends on the depth Froude number as seen in Figure 4(b) [3]. The values of δ, which were calculated by coupling the ship length L from AIS data with the bathymetry H from GEBCO, are larger than 1 as seen in Figure 10. For that reason, angles higher than 19.47° are expected. Ranging from a bit higher for low values of Fr_H (up to 0.5) to close to 90° for Fr_H close to 1. The mean Kelvin angle $\bar{\beta}$ is plotted against both the water depth H (from GEBCO) and the depth Froude number Fr_H (which depends on the water depth from GEBCO and ship speed from AIS data), see Figure 17.

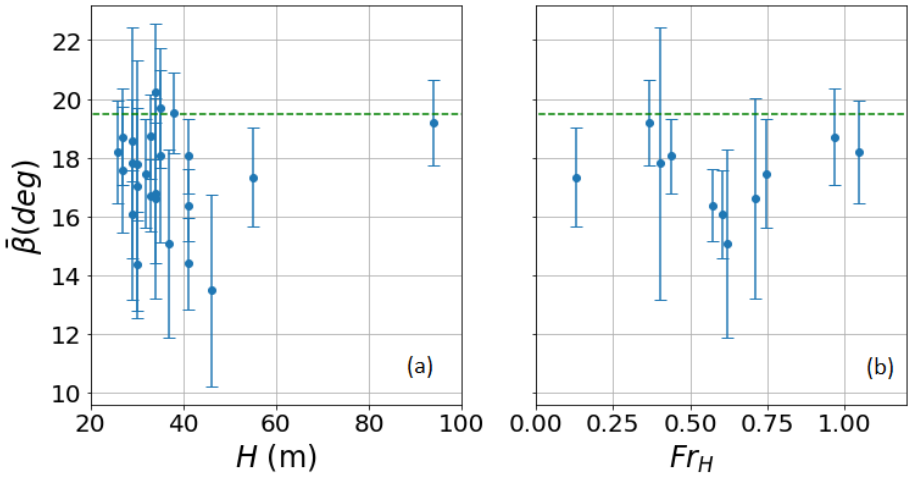

Figure 17: (a): Mean Kelvin angle $\bar{\beta}$ as a function of the water depth H (obtained from GEBCO) based on 26 ship images is displayed in blue. (b): Mean Kelvin angle $\bar{\beta}$ as a function of the depth Froude number Fr_H based on 11 ship images is displayed in blue. The reduction in amount of data points is a result of the dependence on AIS data, which was only coupled successfully in 11 images. In (a) and (b) the theoretical value for the Kelvin angle of 19.47° is displayed as a dashed green line.

The data points in Figure 17(a) are clustered together at water depths ranging from $25 - 55$ meters, with a single outlier close to 100 meters. The mean Kelvin angles are lower than the theoretical angle in almost every ship image, as was already seen in Figure 14. Only two angles are higher than 19.47°, unlike what was expected on basis of Pethiyagoda et al. Figure 17 further illustrates that the depth Froude number does not influence the Kelvin angle such as theoretically predicted; even the Fr_H values very close to $Fr_{H,\mathrm{crit}} = 1$ do still display mean Kelvin angles smaller than 19.47°, where they were expected to rise to values close to 90°. Also, the Kelvin angles do not seem to indicate a trend in Figure 17(a); for different depths both relatively high and low mean Kelvin angles are found. So, in contradiction to Pethiyagoda et al. (2015) no effect of the water depth H is detected.

6.2.2 Mean Kelvin wake angle dependence on wind and current

The wind and current are two environmental variables that depend on direction and are thus vectors. A possible effect on the Kelvin angle can therefore be caused by either the strength of the vector or by its angle with respect to the ship heading θ, which is defined as the difference between the ship heading γ_{ship} and the heading of e.g. the wind vector γ_{wind} . The angle θ is visualised in Figure 18.

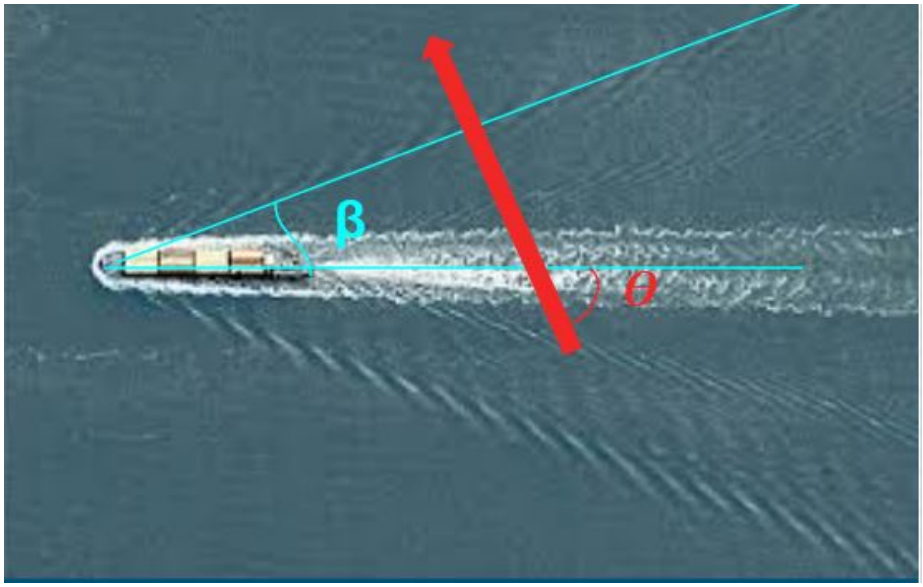

Figure 18: Definition of Kelvin angle β and angle between ship direction and environmental vector θ.

The wind data is modelled data from ERA5, the current is gained both from ERA5 data and observationally determined from Sentinel-2 imagery. The wind heading and current heading may correlate, which is investigated in Figure 19.

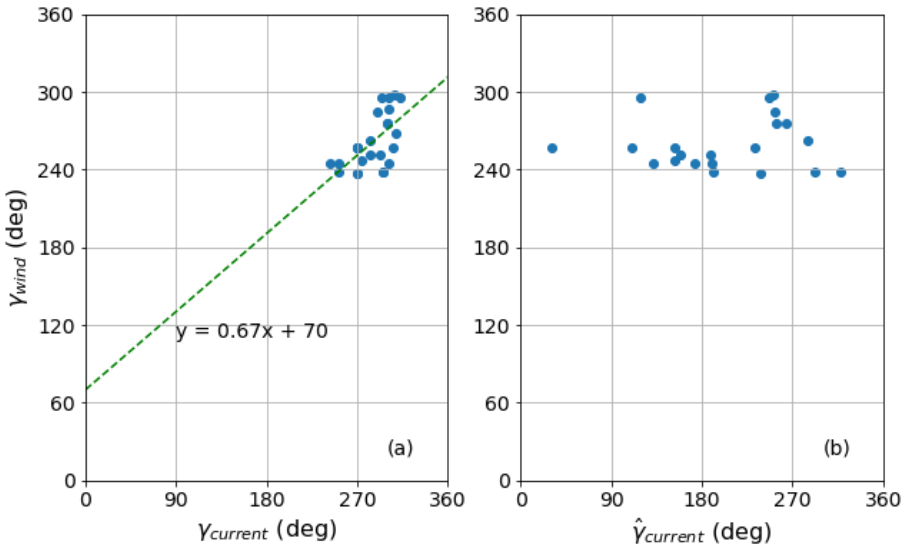

Figure 19: (a): Wind heading γ_{wind} as a function of the modelled current heading γ_{current} for 25 data points is shown in solid blue dots. The linear relation between the two variables is displayed as a dotted green line. The formula of this line is $y = 0.67x + 70$ with r=0.61. (b): Wind heading γ_{wind} as a function of the observed current heading from Sentinel-2 images $\hat{\gamma}_{\text{current}}$ for 25 data points is shown in solid blue dots.

From Figure 19(a) it is seen that the wind heading and current heading from ERA5 are correlated. The current heading determined from Sentinel-2 imagery $\hat{\gamma}_{\text{current}}$ does not depend on the wind heading γ_{wind}, which can be seen in Figure 19(b) from the highly varying angles for $\hat{\gamma}_{\text{current}}$ at a relatively constant wind heading γ_{wind} in the range 240° - 300°. So, when the current is determined from Sentinel-2 imagery no correlation is found.

As the modelled wind heading and modelled current heading are correlated, while the modelled wind heading and observationally determined current heading do not, this suggests that the two different methods of current heading determination do not correlate. This is confirmed in Figure 20; the whole parameter space of $\hat{\gamma}_{\text{current}}$ is reached for only a limited range of γ_{current}.

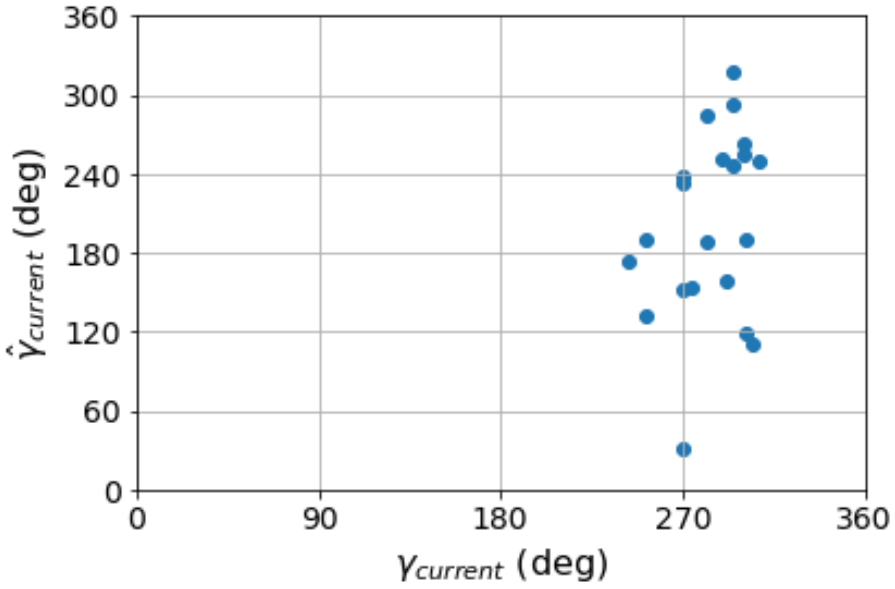

Figure 20: Observationally determined current heading $\hat{\gamma}_{\text{current}}$ as a function of ERA5 current heading γ_{current} for 25 data points.

For only a limited spread in γ_{current} from 240° - 300° a large spread in $\hat{\gamma}_{\text{current}}$ was found, ranging from 30° - 330°. So, a wide spread in $\hat{\gamma}_{\text{current}}$ is found for only limited variety in γ_{current}. As both variables describe the surface current, a correlation of the form $y = x$ would be expected, which is not seen in Figure 20. These findings support the hypothesis that the currents found from ERA5 and from Sentinel-2 observations do not agree well and are not correlated.

Theoretically, a shear flow of uniform vorticity influences the Kelvin wake angle [4]. It is hypothesised that a surface current has an influence on the Kelvin wake angle similar to a shear flow; a current perpendicular to the ship heading causes an asymmetry in the Kelvin wake, where a head-on current would decrease the Kelvin angles on both sides of the wake.

If this hypothesis would be true, the Kelvin wake angle would vary with the angle between the current heading and ship heading θ_{current}. Looking purely at a single Kelvin wake angle, not at the asymmetry, it is expected that $\theta_{\text{current}} = 0°$ leads to small Kelvin angles and $\theta_{\text{current}} = 180°$ leads to large Kelvin angles. Investigating the effects of a non-parallel surface current is difficult, because in most of the ship images (19 out of 26) only a single arm of the Kelvin wake is seen. This is made more difficult by the fact that in the observational determination of the Kelvin angles it is not included on what side the Kelvin arm was measured.

Only looking at the current strength does not tell much, as the direction is also necessary to determine the expected effect. Only looking at the direction of the current could verify that a parallel current affects the Kelvin angle. So, the mean Kelvin angle $\bar{\beta}$ is plotted as a function of both the angle between the modelled current heading and ship heading θ_{current} and as a function of the angle between the observationally determined current and the ship heading $\hat{\theta}_{\text{current}}$, which is displayed in Figure 21.

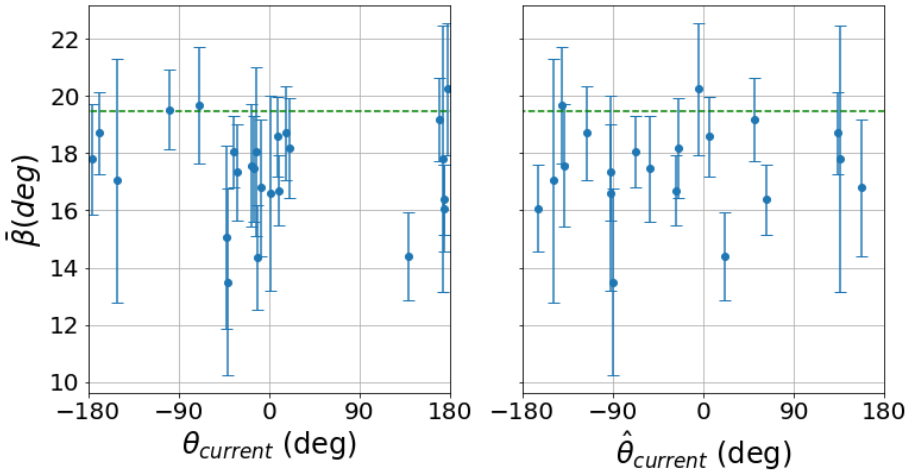

Figure 21: (a) Mean Kelvin angle $\bar{\beta}$ as a function of the angle between the ship heading and modelled current heading θ_{current} based on 25 measurements is displayed in blue. (b) Mean Kelvin angle $\bar{\beta}$ as a function of the angle between the ship heading and observationally determined current heading $\hat{\theta}_{\text{current}}$ based on 23 measurements is displayed in blue. In both (a) and (b) the theoretical value for the Kelvin angle of 19.47° is displayed as a dashed green line.

In Figure 21(a) it can be seen that there is no data for $20° < \theta_{\text{current}} < 130°$. Also a large amount of the data points is centered around $\theta_{\text{current}} = 0°$, the mean Kelvin angles around this point range from 14° - 19°, around $\theta_{\text{current}} = 180°$ (and around $-180°$ as $180° = -180°$) the mean Kelvin angles range from $16° - 20°$. These finding seems to support the hypothesis that the Kelvin angle are lower around $\theta_{\text{current}} = 0°$ than around $\theta_{\text{current}} = 180°$. However, seen the standard deviation of 2.17° and limited amount of data it can not be fully concluded that this is the case.
In Figure 21(b) it can be seen that the data points are fairly evenly spread over the x-axis. There is not a noticeable trend in the data, so there is no indication that the observationally determined ship-current angle influences the Kelvin angle.

Literature suggest the windward Kelvin angle may decrease in the presence

of wind [5]. It is expected that this effect is the most pronounced if the wind is perpendicular to the ship heading. The mean Kelvin angle is plotted against the angle between the ship heading and wind direction in Figure 22

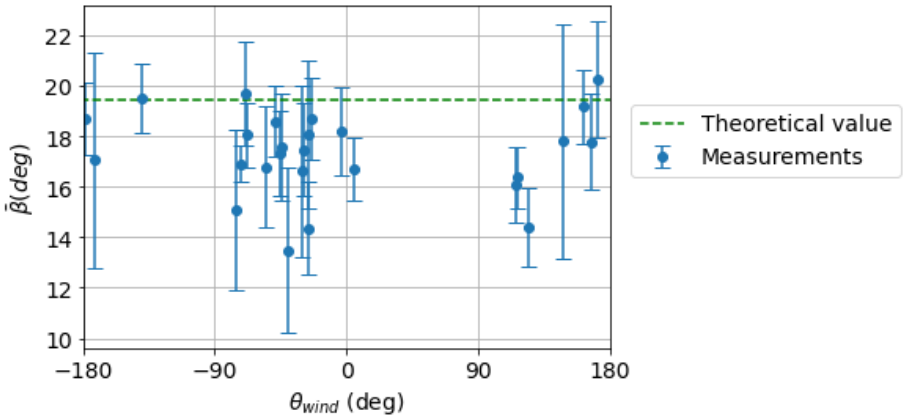

Figure 22: Mean Kelvin angle $\bar{\beta}$ as a function of the angle between the ship and wind θ_{wind} based on 26 measurements is displayed in blue. The theoretical value for the Kelvin angle of 19.47° is displayed as a dashed green line.

As seen in the figure, not all values of θ_{wind} occur, there is next to no data for $0° < \theta_{\text{wind}} < 100°$. Furthermore, it can be noticed that Figure 22 has similarities to Figure 21. There is no clear θ_{wind} which shows a maximum or minimum in the mean Kelvin angle. E.g. in the interval $-90° < \theta_{\text{wind}} < 0°$ it is seen that the Kelvin angle is spread relatively uniformly amongst the ship-wind angles. Based on this data there is no clear influence of the wind on the Kelvin angle.

6.2.3 Mean Kelvin wake asymmetry dependency on wind and current

No clear relation between the mean Kelvin angle and either the wind or current was found. A possibly easier to spot effect is asymmetry in the Kelvin wake. Asymmetry was already shown to cause asymmetry if a shear flow is present [4], so it is hypothesised that a surface current with a component perpendicular to the ship heading causes an asymmetry, as displayed in Figure 23.

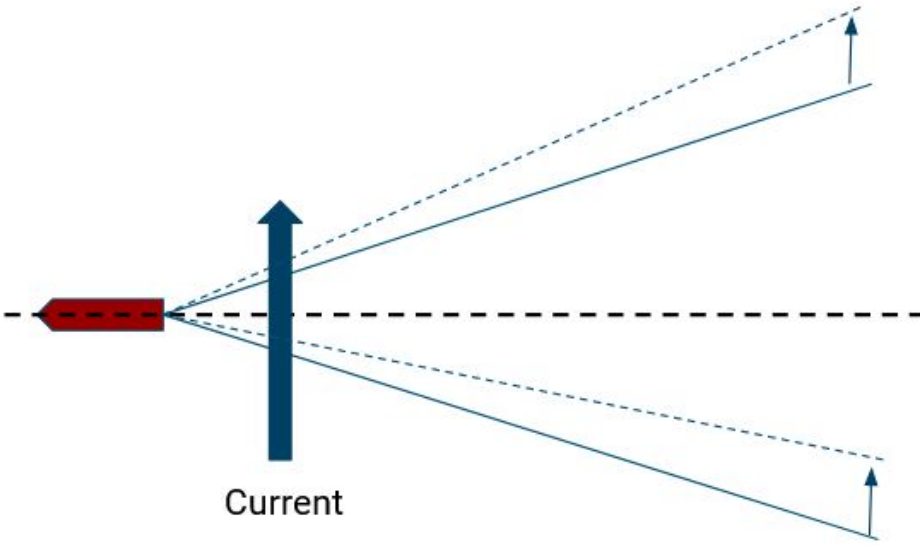

Figure 23: Hypothesised effect of a surface current on the Kelvin wake. The solid blue lines show an uninfluenced, symmetrical Kelvin wake, which might be altered into an asymmetrical Kelvin wake as depicted by the dashed blue lines.

To observationally measure the asymmetry, both arms of the Kelvin wake should be visible. This is the case for only 7 out of 26 of the images ship, reducing the amount of data points.

If both arms of the Kelvin wake are visible, the asymmetry α can be calculated. Here, it is defined as the difference between the Kelvin angle of the left arm β_1 and that of the right arm β_2:

$$\alpha = \beta_1 - \beta_2$$

However, note that more measures for asymmetry can be defined, e.g. the ratio of the two Kelvin angles. The definition of the asymmetry is also visualised in Figure 24.

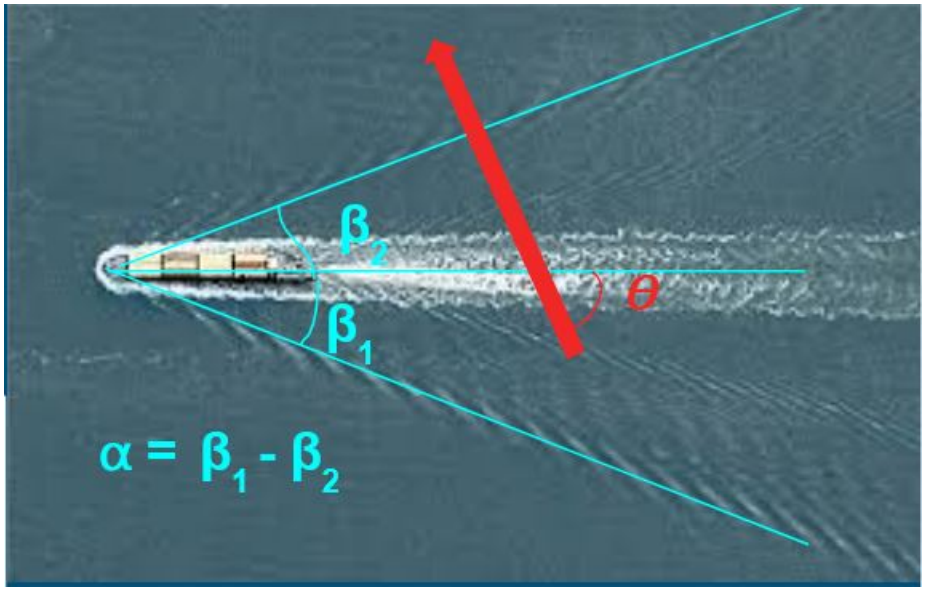

Figure 24: Definition of Kelvin angles β_1 and β_2, angle between ship direction and environmental vector θ (either wind or current) and the Kelvin wake asymmetry α

As the asymmetry is hypothesised to depend on the perpendicular component of the current $c_\perp$, the mean asymmetry $\bar{\alpha}$ is plotted against it. The current was determined twice; once from modelled ERA5 data and once observationally from Sentinel-2 imagery. The asymmetry as a function of the perpendicular components of the currents $c_\perp$ and $\hat{c}_\perp$ is seen in Figure 25.

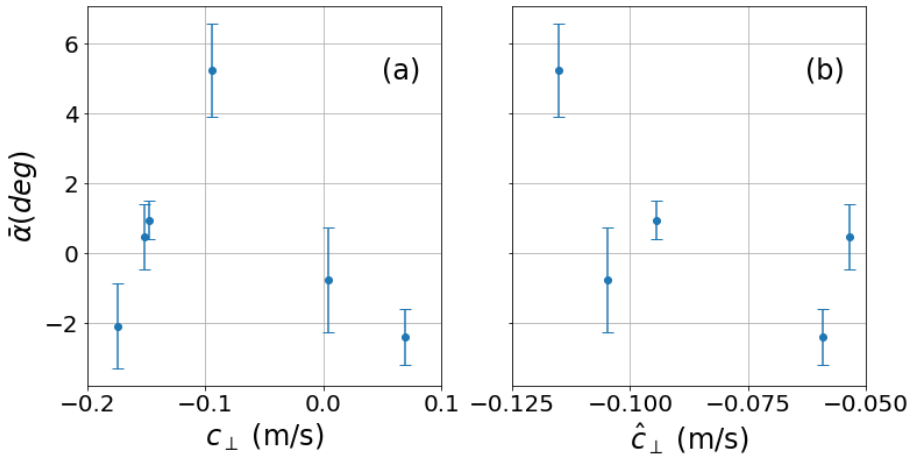

Figure 25: (a): Mean Kelvin angle asymmetry $\bar{\alpha}$ as a function of the perpendicular current component $c_\perp$ based on 6 data points. (b): Mean Kelvin angle asymmetry $\bar{\alpha}$ as a function of the observationally determined perpendicular current component $\hat{c}_\perp$ based on 5 data points.

In Figure 25(a) it can be seen that both positive and negative asymmetry is observed in a range from $-2°$ to $6°$. The surface current velocity is in a range of -0.2 to 0.1 m/s, which are modest current velocities for the ocean (typical surface current velocities are in between 0.05 and 0.5 m/s[67]). A negative $c_\perp$ is a current coming from the right side of a ship and flowing to the left. As a positive asymmetry is associated with a larger left Kelvin arm angle, this would be expected in this case. This is seen at the data point located at $c_\perp = -0.1$. However, at a stronger $c_\perp$ of 0.2 a negative mean asymmetry $\bar{\alpha}$ is found. As the number of data points is also very limited, the hypothesis can not be confirmed from this Figure. It can also be seen that a parabola could be a good fit for this data, although this relation can not be explained from theory. The parabola shape in the data may be a result from the limited amount of data.

In Figure 25(b) it can be seen that only negative values of $\hat{c}_\perp$ were found. On basis of the hypothesis this would be associated with a positive mean asymmetry. For the left most point this is found, but at e.g. $\hat{c}_\perp \approx -0.105$ a negative asymmetry is found. An observation that would support the hypothesis is that the most negative value of $\hat{c}_\perp$ is connected with the highest value of asymmetry. However, the number of data points is very limited and a trend is not clear, so the hypothesis can not be confirmed on basis of this data alone.

Also, it is hypothesised that the perpendicular component of the wind can influence the Kelvin angle asymmetry according to Figure 23 [5]. The effect of the of the perpendicular component of the ERA5 modelled wind $w_\perp$ is displayed in Figure 26.

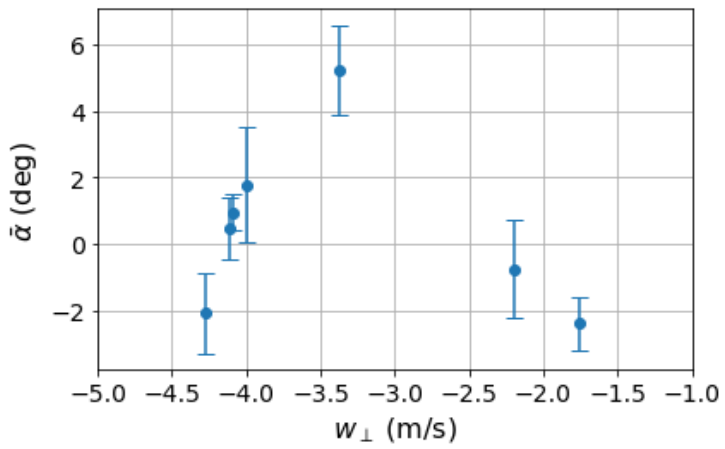

Figure 26: Mean Kelvin angle asymmetry $\bar{\alpha}$ as a function of the perpendicular component of the wind $w_\perp$ based on 7 measurements.

What can be seen in the preceding figure is that asymmetry is present in a range from -2° to 6°. Only wind approaching from the left of the ships (negative $w_\perp$) is observed, which is in a range of -4.5 to -1.7 m/s (gentle breeze on scale of Beaufort). On basis of the hypothesis, this should result in positive asymmetry. This is found for some of the ships, but a negative asymmetry is also found. Furthermore, it can also be observed that the figure resembles Figure 25 quite well, which can be expected on basis of the correlation between $c_\perp$ and $w_\perp$. This also means that a parabola might be fitted through the data points found, although there would be no theoretical explanation for that fit. Partially because of the limited amount of data, the hypothesis that a positive asymmetry is caused by a negative perpendicular wind component can not be confirmed.

7 Discussion

7.1 Error in Kelvin angle measurement

Kelvin angles were successfully determined from Planet imagery. Interestingly, the angles show deviations from the theoretical Kelvin angle value of 19.47°. However, the deviations in Kelvin angle are also not as expected by different earlier studies [2][4][3]. Due to presence of a measurement error in the Kelvin angle determination deviations could be the result of noise caused by the error. This would then explain the discrepancy between the Kelvin angles determined in this study and the expected angles. So, it has to be determined whether noise induced by the measurement error could cause the observed deviations from theory.

The mean Kelvin angles that were calculated from the Planet images deviate from the theoretical base value of 19.47° and the mean standard deviation is 2.2°. This mean standard deviation $\bar{\sigma}$ is used as a proxy for the measurement error. To investigate the cause of the deviations Figure 14 is repeated here as Figure 27.

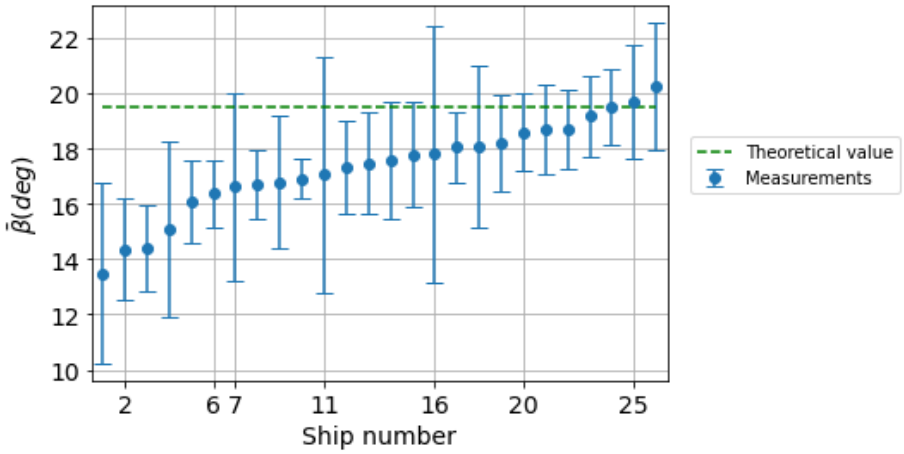

Figure 27: The mean Kelvin angle $\bar{\beta}$ and its standard deviation σ of 26 images determined using 12 contributions per image, where the 12 contributions are from 4 different persons. The theoretical value for the Kelvin angle of 19.47° is displayed as a dashed green line.

What can be seen in Figure 27 is that the theoretical Kelvin angle is in some cases within 1 standard deviation of a measured point, e.g. at ship numbers 7, 11 and 16. The error is then large enough to explain the deviation from 19.47°; the deviating Kelvin angle could then be explained purely as a measurement error.

However, other points do seem to show a deviation that can not be explained

by their measurement error. Ship numbers 2 and 6 do both show a smaller than expected Kelvin angle. The standard deviation associated with these points is relatively small, as a result the deviation can not be explained by this error estimate alone.

Even tough the measurement error does play a role, e.g. ship numbers 2 and 6 show that actual deviations of the Kelvin angle were found, not just measurement induced noise.

Furthermore, the measured standard deviation is not the same for every ship, as seen in Figure 27. Somehow, the standard deviation is as low as $\sim 0.8^\circ$ (ship number 10) for a ship and as high as $\sim 4^\circ$ (ship number 16).
This noticeable difference may be caused by a few different things:

- In some cases, a Kelvin wake can be seen at both the bow and stern. Both can be used to calculate a Kelvin angle, which can result in two different values of the Kelvin angle. This would then cause a larger spread in the measured angles. An example of a ship displaying both a bow and stern Kelvin wake is seen in Figure 28.

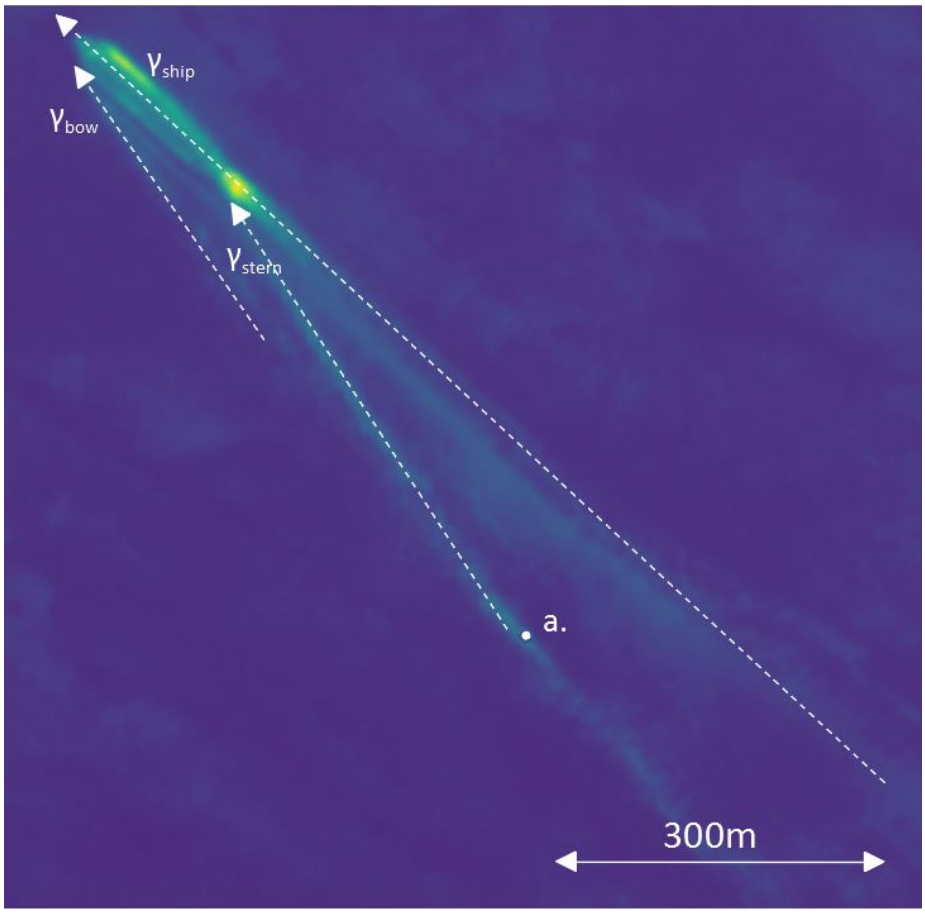

Figure 28: 3 meter pixel resolution Planet image cutout of a ship displaying Kelvin wake formation at both the bow and stern. The ship was observed on 10-4-2020 at 11:25 Singapore time, it was located at 103.41°N, 1.25°E. The heading of the ship γ_{ship} and the slightly differing headings of the bow and stern Kelvin wake γ_{bow} and γ_{stern} are seen. Point a. shows a kink in the wave pattern, which could be the result of the ship turning.

- In 7 out of the 26 analyzed ship images the Kelvin wake is seen at both sides of the ship. Only if the wake is symmetrical both Kelvin angles would be the same. Asymmetry is present however, so measuring the Kelvin angle from both arms interchangeably leads to more spread in the measured angle.
- The image quality can make it harder to determine the direction of the Kelvin wake and thus the Kelvin angle. This again increases the spread in measured angles.

Both the bow and stern waves and the different Kelvin arms could lead to measurements centered around two different values. So, the angles may show a bimodal distribution; the data could be centered around two different mean values, as two different data distributions may be present. Such a pattern could become visible if all measured angles are shown, as in Figure 29.

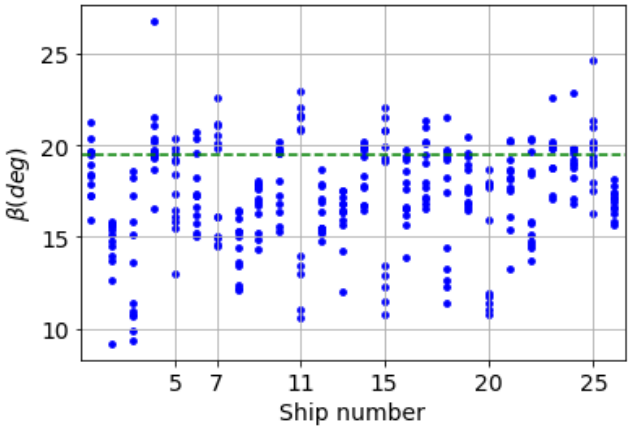

Figure 29: The Kelvin angle β of 26 images determined using 12 contributions per image. The theoretical value for the Kelvin angle of 19.47°is displayed as a dashed green line.

By looking at the preceding figure, measurements at ship numbers 7, 11, 15 and 20 seem to indicate a bimodal distribution; two groups of measurements centered around different Kelvin angle values.
As a more rigid test of bimodality the 12 measurement per ship are divided into two groups by fitting the data to a Gaussian mixture model. By definition the data is then divided into two groups, which does not provide any information yet. Based on the fitted distribution an estimation of the probability that a measurement belongs to each of the two groups can be made. For example, a point could have a 99% probability of belonging to group 1 (and consequently a 1% chance of belonging to group 2), that data point would then suggest a bimodal distribution. On the contrary, if a point has a 50% probability to belong to both group 1 and group 2 the data is unlikely to be bimodal. To estimate whether the data for a single ship is bimodal the following criterion is used: *The distribution is bimodal if every data point in the data set can be allocated to a group with at least 90% probability.* Based on this definition the Kelvin angle measurement of 19 of the 26 ships seems to be influenced by bimodality in the data.

So, for these 19 measurements the relatively large error could be explained by the data having a bimodal distribution. By defining more precisely what Kelvin wake should be measured, e.g. the bow Kelvin wake situated at the

left side of the ship, this measurement error can be reduced for a large part of the data. Some of the ships do not clearly display a bimodal distribution, the error is then more likely to be the result of a limited image quality coupled with difficulty in having consistent measurements.

7.2 Explanation of Kelvin angle deviations

Kelvin angle deviations were expected on basis of theory.

Based on Rabaud et al. (2013) no deviations were expected on basis of high hull Froude numbers (seen for small, fast ships)[2]. Smaller than expected Kelvin angle were found, but no contribution based on the ship length was found. The absence of an influence of the ship length is as predicted for the observed ships. Therefore, the deviations in the Kelvin angle are not expected or explained by Rabaud et al. (2013).

Based on Pethiyagoda et al. (2015) Kelvin angles larger than 19.47° were expected due to limited water depth [3]. Only a few cases were found where the mean Kelvin angle $\bar{\beta}$ is larger than the theoretical value. The largest part of the measured Kelvin angles were 19.47° or less, which is not as expected on basis of the water depth at the observed ships. Pethiyagoda et al. (2015) is a model study; the results are not based on observations. The difference between the expected and measured Kelvin angles might be explained by incorrect assumptions in the model. For example, a simple axisymmetric pressure distribution is assumed in theory, which may not cause the ship wave patterns as seen in observations.

Ellingsen (2014) models an asymmetric Kelvin wake as a result of a side-on shear [4]. In this research asymmetry was found in the presence of a surface current, but not in the manner as expected from the hypothesis; the direction of the surface current does not seem to influence the direction of the asymmetry. The unexpected behaviour could be the result of a wrong hypothesis. It was hypothesised that a side-on current may have the same effect on the Kelvin wake as a side-on shear flow of constant vorticity, which may be an oversimplification. Furthermore, Ellingsen (2014) is again a modelling study. This could result in some processes influencing the Kelvin angle not being included or being simplified in order to model it.

Finally, Noblesse et al (2014) shows the influence of interference of ship wakes on the Kelvin angle [52]. It is stated that for ships with a small hull Froude number, which is the case in the observations in this research, the Kelvin angles are in the range $13° < \beta < 21°$. This range of Kelvin angles agrees quite well with the observationally found Kelvin angles as seen in e.g. Figure 27. To be more precise; the interference of the bow and stern waves could cause constructive interference for certain unfavourable hull Froude numbers. The angle of the

highest intensity observed wave β_{app} due to interference is given by:

$$\beta_{\text{app}} = \arctan\Big(\frac{\sqrt{(2n-1)^2\pi^2\text{Fr}_L^4/l^2 - 1}}{2(2n-1)^2\pi^2\text{Fr}_L^4/l^2 - 1}\Big) \tag{10}$$

where l is a dimensionless value for the distance between the source of the bow and stern waves relative to the ship length of 0.9, n is an integer that is the amount of wavelengths difference between the two waves leading to interference and Fr_L is the hull Froude number.

Equation 10 has no solutions for the low hull Froude numbers found in this study unless n takes on high values (for $n = 10$ a solution is found in 4 out of 11 cases), as the square root in equation 10 should contain a positive number, which is not the case for low values of the variables n and Fr_L. Only for $n = 179$ solutions are found for all hull Froude numbers calculated in this research. The apparent Kelvin wake angles β_{app} predicted by Noblesse et al. (2014) are compared to the measured angles $\hat{\beta}$ in Table 1.

β_{app} (deg)	$\hat{\beta}$ (deg)	Δ(deg)
10.07	17.46	7.38
19.32	18.18	1.13
11.64	17.80	6.15
16.03	16.36	0.34
13.81	16.07	2.26
4.308	17.33	13.02
17.46	18.71	1.24
17.46	16.61	0.84
13.51	18.05	4.53
18.41	15.07	3.34
10.45	19.1	8.73

Table 1: Comparison of predicted Kelvin angle by Noblesse et al. (2014) and measured Kelvin angle in this study.

The difference between the predicted and observed Kelvin angles Δ in Table 1 is large. However, the predicted angles do generally fall within the same range as the observed angles. So, a precise prediction on basis on interference is not possible using equation 10.

Nonetheless, the described range of angles agrees with the range of observed Kelvin angles. So, an influence of interference on the observed Kelvin angles seems very plausible.

7.3 Bias in environment

The study area was limited to the Strait of Singapore. However, this may increase the difficulty of finding out what effects the Kelvin angle. The Kelvin angle was coupled to different environmental variables. However, as a result of only investigating the Kelvin angle within a local region, the environmental variables show a preference with a limited spread in the displayed values. The sea surface temperature does for example stay within a range of 302K - 303K. This limited spread makes it harder to find relations in the data, because the influence of only a small difference in a variable will likely only have a limited influence on the Kelvin angle. A small difference in the Kelvin angle can be hard to detect, as the measurement error is substantial.

Except for the temperature, the wind heading and surface current heading determined from the ERA5 reanalysis show a strong preference for certain directions, limiting the coverage for these variables. The preference for headings is displayed in Figure 30. This is a strong contrast with modelling studies, where the parameter space can be fully explored.

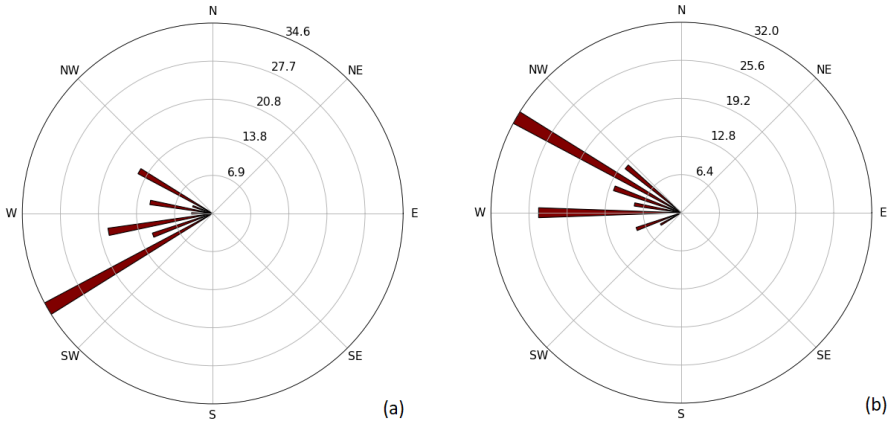

Figure 30: (a): Rose plot displaying the wind heading at the locations of the imaged ships, gained from the ERA5 reanalysis. A longer line visualises that heading is found more often in the data. (b): Rose plot displaying the surface current heading at the locations of the imaged ships, gained from the ERA5 reanalysis. A longer line visualises that heading is found more often in the data.

It can be seen that the ERA5 wind is predominantly to the West, just like the ERA5 surface current, again showing limited spread. The surface current was also observationally measured, using Sentinel-2 imagery. In this alternate way of determining the surface current there is more variety in the surface current heading, as seen in Figure 31.

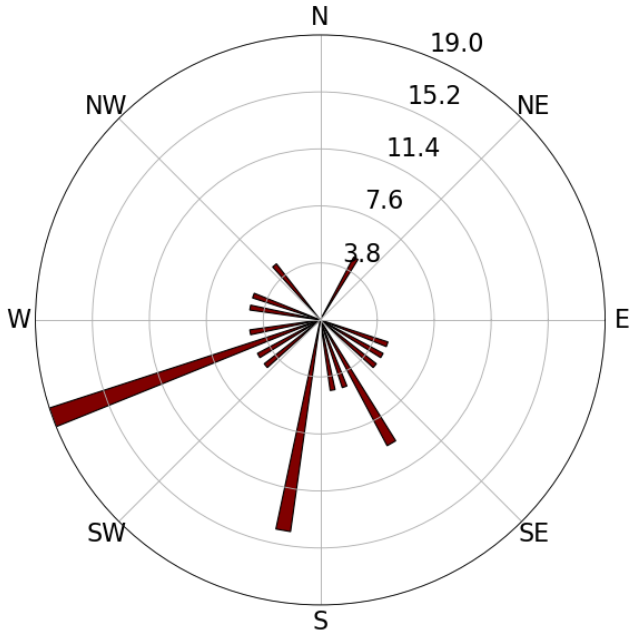

Figure 31: Rose plot displaying the surface current heading at the locations of the imaged ships, gained from Sentinel-2 images. A longer line visualises that heading is found more often in the data.

The different surface currents raise the question: *'Which surface current is realistic?'*. Based on a difference in resolution, the surface current from Sentinel-2 images seems more reliable. The ERA5 data has a grid resolution of 30km by 30km, so it displays an average value over this area. The Sentinel-2 data is measured more locally from the direction of individual swell waves in a 640m by 640m area.

7.4 Bias in visibility

Not only the environmental variables show limited spread. The ship heading also shows preference for certain directions, as seen in Figure 32.

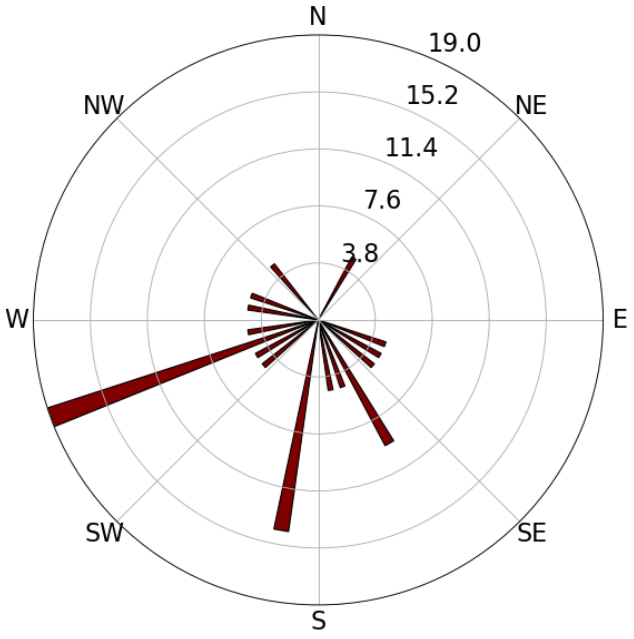

Figure 32: Rose plot displaying the ship headings, gained from Planet images. A longer line visualises that heading is found more often in the data.

On one hand this bias for ship directions may be caused by the shipping routes in the strait of Sinagpore. Ships can travel in all directions, but the cargo ships that can easily be seen in Planet data predominantly do so along the directions of shipping routes.
On the other hand a bias may also be caused by the visualisation requirements of the Kelvin wake. The visibility of a Kelvin wake depends on measurement geometry as seen in section3.2.1; only under specific conditions is the Kelvin wake visible through specular reflection. The Planet images used are all taken at the end of the morning. As a result the sun zenith and azimuth angles are expected to be quite constant. Also, the satellite zenith and azimuth angles are relatively constant. All in all a preference for certain ship headings is created by the requirements for visualisation of the Kelvin wake.

8 Conclusion

In this research it was shown that Kelvin angles can be measured from optical Planet satellite images. The found Kelvin angles were successfully coupled to AIS Spire data, ERA5 reanalysis data, GEBCO bathymetry data and surface current data obtained from Sentinel-2.

Measurements by the author were done with a relatively low standard deviation (which is a proxy for the measurement error) of 0.7°. However, multiple visible Kelvin wakes at either the bow and stern or left and right side of the ship lead to multiple possible interpretations of the Kelvin angle; if multiple persons measure the standard deviation Kelvin angle increases to 2.2°, which can be explained by the fact that it was not strictly described what Kelvin angle should be measured if multiple are present. The systematic error in the Kelvin angle measurement is estimated at 0.32° and thus plays a lesser role compare to the measurement error.

The observation of Kelvin wakes is determined by its visibility through specular reflection. In combination with the limited area that is investigated a bias in the data is created.

The measured Kelvin angles show a spread between 13° and 21°, deviating from the theoretical Kelvin angle of 19.47°. Explanations were hypothesised on basis of theoretical studies, but influences from ship length, water depth, wind and current are not as predicted. Interference of the bow and stern Kelvin wakes is likely to influence the Kelvin angle deviation, although the Kelvin angles can not be predicted from the theoretically described interference yet.

The shape of the pressure distribution (shape of the ship) is often simplified in literature, which may ignore effects of e.g. interference, that is shown to effect the Kelvin wake formation.

Finally, asymmetry was observed in Kelvin wakes. The wind and surface current were hypothesised to determine the amount of asymmetry, but this could not be confirmed from the data.

9 Perspectives

Future research could use the findings of this research as a basis for further development. First of all, the measurement procedure could be looked at and improved upon. A straightforward improvement could be made by strictly prescribing what Kelvin angle is measured. E.g. if a bow and stern Kelvin wake is visible prescribing that only the stern wake is measured will likely decrease the measurement error. Also, the error is likely to decrease if the pixel resolution of images increases, which will likely become more available in the future.

Furthermore, more wake angle measurements could be collected to have a stronger statistical base to draw conclusions from. Naturally this will happen as the pixel resolution of images will likely increase with time, which will increase the visibility of the Kelvin wake in imagery [7].

To further increase the amount of data the currently time-consuming process of determining the Kelvin angle could be automatized to a large degree. AIS data could be taken as a base: satellite imagery can be coupled to this data. It was already shown in literature that ship wakes can be automatically detected using a Radon transform [7], which would be an important step in automatically measuring the Kelvin angle. While a full automatisation would be ideal, it is not easy to accomplish, seen the amount of steps that have to be taken. The steps that are taken can be summarized as:

- Finding ships displaying a Kelvin wake in optical satellite imagery. Automatisation of ship and wake detection have been described before in a study of optical Sentinel-2 imagery [26]. A study focused at ship-iceberg discrimination in Sentinel-2 imagery is available and may be helpful if measurements further from the equator are performed [27]. An alternative ship detection method in optical imagery is described in Xu et al. (2017) [58]. An overview of ship detection methods in optical imagery was performed by Kanjir (2018) [50].

- Measuring the Kelvin angle displayed in images. Using a Radon transform could be helpful; this transform can be used to detect straight lines and their orientation, a property that has been used to detect ship wakes for SAR images [59]. In optical imagery the Radon transform can, in similar fashion as for SAR images, extract the direction of lines. If the orientation of the ship and Kelvin arms can be extracted the Kelvin angle can be calculated from those orientations.

- Coupling imagery to ship data using AIS. This was partly automatised in this project. An example of full automatisation is seen in Kurekin et al. (2019) [55]. An important difference with the AIS coupling in this project is the interpolation, Kurekin et al. (2019) uses a more complex spline interpolation using multiple AIS points to determine a ship's track.

In contrast, this research uses linear interpolation based on a single AIS data point.

- Coupling imagery to oceanic data is likely the most straightforward step to automatise. The main challenge is automatically downloading the correct data set for an image, but this could be done using the API of different data sources. The coupling could be made more simply based on the position and data that has the smallest time difference with the ship image.

It is expected that automatising all steps in succession is not easy, some steps can be automatised relatively straightforward to reduce the time taken to get data that can be analyzed.

Additionally, the used pressure distribution (how the ship is modelled) seems to be limiting the understanding of the Kelvin wake. The effect of more realistic ship shapes could be modelled and tested against observations to improve the understanding of interference. The recent theoretical work of Colen et al. (2021) could be taken as a basis for future research [57].

Also, a different approach to measuring the Kelvin angle could be explored. A theoretical study showed that visible-light polarisation can be used to image wakes, which could be utilised in further research [33].

Finally, current literature isolated the influence of a single parameter on the Kelvin wake. In observations it is possible that multiple factors alter the Kelvin angle. Therefore it would be interesting to investigate the Kelvin angle under conditions were multiple described factors causing Kelvin angle deviations are present, although this is expected to be challenging.

10 Acknowledgements

I'd like to thank Planet for the access we received to their satellite imagery archive, as well as Spire for the access they gave to their AIS database.

Writing a thesis in times of Covid is not an easy task, luckily the Climate Physics study group was there to make this easier. To Luke Bohn, Lena Buth, Emma Griffin, Handi Liu, Sophie Schmiz and Julia Weiffenbach: I am really happy to have joined you in the study group. I enjoyed our '15 minute' breaks and the help and motivation you gave me for my thesis.

I'd also like to thank Neha Mahendale and Ewout Melman for their company in the Master room and the coffee breaks. It was amazing to be able to see you in a time of social distancing.

Finally, special thanks to Bas Altena for all the provided help. Help on the thesis by explaining and giving feedback, but also help in dealing with the stress of writing. I appreciate the time you took for our meetings.

References

[1] W. Thomson (1904). *Deep Sea Ship-Waves*. pp. 1060-1084. Proceedings of the Royal Society of Edinburgh.

[2] M. Rabaud and F. Moisy (2013). *Ship Wakes: Kelvin or Mach Angle?* Physical Review Letters **110**.

[3] R. Pethiyagoda et al. (2015). *Wake angle for surface gravity waves on a finite depth fluid* Phys. Fluids **27**.

[4] S. Å. Ellingsen (2014). *Ship waves in the presence of uniform vorticity*. Journal of Fluid Mechanics **742**.

[5] M. Fang et al. (2011). *Kelvin Ship Wake in the Wind Waves Field and on the Finite Sea Depth*. Journal of Mechanics **27**.

[6] I. Shugan (2008). *Kelvin Ship Wake Modification due to Wind Waves*. Journal of Ocean Engineering and Technology **22**.

[7] Y. Liu and R. Deng (2018). *Ship Wakes in Optical Images*. Journal of Atmospheric and Oceanic Technology **35** pp. 1633-1648.

[8] W. Esaias et al. (1998). *An Overview of MODIS Capabilities for Ocean Science Observations*. IEEE Transactions on Geoscience and Remote Sensing **36**.

[9] H. Youbin et al. (2008). *Characteristics of internal-wave and internal-tide deposits and their hydrocarbon potential*. Pet. Sci. **5**.

[10] C. Jackson (2007). *Internal wave detection using the Moderate Resolution Imaging Spectroradiometer (MODIS)*. JGR Oceans **112**.

[11] C. Hu et al. (2009). *Detection of natural oil slicks in the NW Gulf of Mexico using MODIS imagery*. Geophysical research letters **36**.

[12] F. Su et al. (2007). *Estimating amplitudes of internal waves using satellite ocean colour imagery of the South China Sea*. International Journal of Remote Sensing **36**.

[13] S. Li et al. (2009). *Ocean color products retrieval and validation around China coast with MODIS*. Acta Oceanol. Sin. **29**.

[14] M. Wang (2007). *MODIS-derived ocean color products along the China east coastal region*. Geophysical Research Letters **34**.

[15] M. Adamo et al. (2006). *On the combined use of sun glint Modis and Meris signatures and SAR data to detect oil slicks*. Remote Sensing of the Ocean, Sea Ice, and Large Water Regions, 63600G.

[16] C. Hu et al. (2009). *Detection of natural oil slicks in the NW Gulf of Mexico using MODIS imagery*. Geophysical research letters **36**.

[17] B. Liu et al. (2019). *Oceanic Internal Waves in the Sulu–Celebes Sea Under Sunglint and Moonglint.* IEEE Transactions on Geoscience and Remote Sensing **57**.

[18] N. Nezlin et al. (2008). *Stormwater plume detection by MODIS imagery in the southern California coastal ocean.* Estuarine, Coastal and Shelf Science **80**.

[19] A. Kubryakov et al. (2021). *Application of Landsat imagery for the investigation of wave breaking.* Remote Sensing of Environment **253**.

[20] A. Iqbal et al. (2018). *Identification and mapping of coral reefs using Landsat 8 OLI in Astola Island, Pakistan coastal ocean.* 14th International Conference on Emerging Technologies (ICET)

[21] P. Jagalingam et al. (2017). *Estimation of bathymetry along the coast of Mangaluru using Landsat-8 imagery.* International Jounral of Ocean and Climate Systems **8**.

[22] P. Jagalingam et al. (2015). *Bathymetry Mapping Using Landsat 8 Satellite Imagery.* Procedia Engineering **116**.

[23] R. Abileah (2009). *Surveying coastal ship traffic with Landsat.* Oceans 2009 pp. 1-6.

[24] A. Osadchiev et al. (2019). *Spreading dynamics of small river plumes off the northeastern coast of the Black Sea observed by Landsat 8 and Sentinel-2.* Remote Sensing of Environment **221**.

[25] M. Yurovskaya et al. (2019). *Ocean surface current retrieval from space: The Sentinel-2 multispectral capabilities.* Remote Sensing of Environment **234**.

[26] H. Heiselberg. (2016). *A Direct and Fast Methodology for Ship Recognition in Sentinel-2 Multispectral Imagery.* Remote Sensing **8**.

[27] P. Heiselberg and H. Heiselberg (2017). *Ship-Iceberg Discrimination in Sentinel-2 Multispectral Imagery by Supervised Classification.* Remote Sensing **9**.

[28] Y. Liu et al. (2021). *A novel technique for ship wake detection from optical images.* Remote Sensing of Environment **258**.

[29] J. Shin (2021). *High Spatial-Resolution Red Tide Detection in the Southern Coast of Korea Using U-Net from PlanetScope Imagery.* Sensors **21**.

[30] B. Gabr (2020). *PlanetScope and Landsat 8 Imageries for Bathymetry Mapping.* J. Mar. Sci. Eng. **8**.

[31] F. Lei (2019). *Ship Extraction using Post CNN from High Resolution Optical Remotely Sensed Images*. 2019 IEEE 3rd Information Technology, Networking, Electronic and Automation Control Conference.

[32] F. Xue et al. (2020). *Wake Features of Moving Submerged Bodies and Motion State Inversion of Submarines*. Digital Object Identifier 10 **10**.

[33] F. Xue et al. (2021). *Airborne optical polarization imaging for observation of submarine Kelvin wakes on the sea surface: Imaging chain and simulation*. Photogrammetry and Remote Sensing **178**.

[34] A. Arnold-Bos et al. (2007). *Obtaining a ship's speed and direction from its Kelvin wake spectrum using stochastic matched filtering*.2007 IEEE International Geoscience and Remote Sensing Symposium.

[35] G. Zilman et al. (2004). *The Speed and Beam of a Ship From Its Wake's SAR Images*. IEEE transtactions on geoscience and remote sensing **42**.

[36] M. Krishnaveni et al. (2009). *An optimal method for wake detection in SAR images using Radon transformation combined with wavelet filters*. International Journal of Computer Science and Information Security **6**.

[37] I. Hennings et al. (1999). *Radar imaging of Kelvin arms of ship wakes*. International Journal of Remote Sensing **20**.

[38] A. Panico et al. (2017). *SAR-Based Vessel Velocity Estimation From Partially Imaged Kelvin Pattern*. IEEE Geoscience and Remote Sensing Letters **14**.

[39] M. Graziano et al. (2017). *Performance Analysis of Ship Wake Detection on Sentinel-1 SAR Images* Remote Sensing **9**.

[40] G. Palubinskas et al. (2009). *Joint use of optical and SAR data for ship detection*. Conference paper on Workshop on SAR Ocean Remote Sensing Ocean SAR.

[41] ESA. Sentinel-1 SAR overview found at `https://sentinel.esa.int/web/sentinel/user-guides/sentinel-1-sar/overview`.

[42] ESA. Sentinel-2 overview found at `https://sentinels.copernicus.eu/web/sentinel/missions/sentinel-2/overview`.

[43] C. Cox et al. (1954). *Measurement of the Roughness of the Sea Surface from Photographs of the Sun's Glitter*. J. Opt. Soc. Am. **44**.

[44] D. Wang et al. (2019). *On Optimal Imaging Angles in Multi-Angle Ocean Sun Glitter Remote-Sensing Platforms to Observe Sea Surface Roughness*. Sensors **19**.

[45] G. Crapper. (1984). *Introduction to water waves* Chichester, West Sussex, England: E. Horwood.

[46] E. Bergsma et al. (2019). *Radon-Augmented Sentinel-2 Satellite Imagery to Derive Wave-Patterns and Regional Bathymetry* Remote Sensing **11**.

[47] D. Chen et al. (2016). *Estimating ship emissions based on AIS data for port of Tianjin, China* Atmospheric Environment **145**.

[48] F. Xiao et al. (2015). *Comparison study on AIS data of ship traffic behavior* Ocean Engineering **95**.

[49] U. Löptien et al. (2014). *Ice and AIS: ship speed data and sea ice forecasts in the Baltic Sea* The Cryosphere **8**.

[50] U. Kanjir et al. (2018). *Vessel detection and classification from spaceborne optical images: A literature survey.* Remote Sensing of Environment **207**.

[51] A. Darmon et al. (2013). *Kelvin wake patterns at large Froude numbers.* Journal of Fluid Mechanics **738**.

[52] F. Noblesse et al. (2014). *Why can ship wakes appear narrower than Kelvin's angle?.* Europen Journal of Mechanics B/Fluids **46**.

[53] Y. Liu et al. (2019). *Simulation of Kelvin wakes in optical images of rough sea surface.* Applied Ocean research **89**.

[54] Planet. *Planet Imagery Product specification* found at `https://www.planet.com/products/satellite-imagery/files/1610.06_Spec%20Sheet_Combined_Imagery_Product_Letter_ENGv1.pdf`. Page 19.

[55] A. Kurekin et al. (2019). *Operational monitoring of illegal fishing in Ghana through exploitation of satellite Earth observation and AIS Data.* Remote Sensing **11**.

[56] X. Zhang et al. (2004). *Optical influence of ship wakes.* Applied Optics **43**.

[57] J. Colen et al. (2021). *Kelvin-Froude wake patterns of a traveling pressure disturbance.* Phys. Fluid Dynamics **85**.

[58] F. Xu et al. (2017). *A Hierarchical Maritime Target Detection Method for Optical Remote Sensing Imagery.* Remote Sensing **9**.

[59] R. Hansen et al. (1996). *Ship wake detection using Radon transforms of filtered SAR imagery.* Proceedings of SPIE.

[60] M. Svanberg et al. (2019). *AIS in maritime research.* Marine Policy **106**.

[61] H. Saputra et al. (2015). *Estimation of exhaust ship emission from marine traffic in the straits of Singapore and Batam waterways using AIS data.* Emering and current issues in engineering **77**.

[62] Spire. Spire AIS https://spire.com/spirepedia/automatic-identification-system/.

[63] Gebco. Gridded bathymetry data https://www.gebco.net/data_and_products/gridded_bathymetry_data/#global.

[64] ERA5. ERA5 hourly data on single levels from 1979 to present https://cds.climate.copernicus.eu/cdsapp#!/dataset/reanalysis-era5-single-levels?tab=overview.

[65] A. Kääb et al. (2014). *Motion detection using near-simultaneous satellite acquisitions*. Remote Sensing of Environment **154**.

[66] D. Yang et al. (2019). *How big data enriches maritime research – a critical review of Automatic Identification System (AIS) data applications* Transport Reviews **39**.

[67] A. Gordon et al. (2021). *Ocean current*. Encyclopedia Britannica.

Appendices

A Derivation Kelvin Angle

The derivation starts of with a ship moving with a velocity v, forming transverse waves with make an angle α with the ship and are contained within the Kelvin envelope of angle β.

A ship can be seen as a large disturbance of its surroundings, causing a whole spectrum of waves to form. However, in observations only certain waves are very pronounced; mainly the transverse waves which make an angle α. As there is a large spectrum of waves created, the waves that remain are in some form sustained by the motion of the ship.

To be more precise, the transverse waves are sustained because the phase velocity c_p of the transverse waves equals the component of the ship's velocity parallel to this wave $v\sin(\alpha)$. Mathematically this is denoted as

$$c_p = v\sin(\alpha). \tag{11}$$

using that the phase velocity is defined as $c_p = \frac{\omega}{k}$, where ω is the angular frequency and k the wavenumber. In deep water this wavenumber is given by $\omega = \sqrt{gk}$. Combining these relations with equation 11 leads to

$$k = \frac{g}{v^2\sin^2(\alpha)}. \tag{12}$$

To investigate any constructive interference, the phase of the wave ϕ is considered at a point P, which lays along the Kelvin envelope. So, it makes an angle β with the ship position. The phase at point P is given by

$$\phi = \vec{k}_\alpha \cdot \vec{r} = -kr\sin(\alpha - \beta) \tag{13}$$

where r is the distance from the wave source to point P. Substitute the relation from equation 12 into equation 13 to find

$$\phi = \frac{-gr\sin(\alpha-\beta)}{v^2\sin^2(\alpha)}$$

and take the derivative with respect to α to find

$$\frac{\partial\phi}{\partial\alpha} = \frac{-gr}{v^2}\left(\frac{-\sin^2(\alpha)\cos(\alpha-\beta) + 2\sin(\alpha-\beta)\sin(\alpha)\cos(\alpha)}{\sin^4(\alpha)}\right).$$

The preceding equation can be simplified to

$$\frac{\partial\phi}{\partial\alpha} = \frac{gr}{v^2}\Big(\sin(\alpha)\cos(\alpha-\beta) - 2\sin(\alpha-\beta)\cos(\alpha)\Big) \tag{14}$$

A special case of equation 14 is when $\frac{\partial \phi}{\partial \alpha} = 0$, in this case the phase ϕ does not vary for varying angles α. As a result constructive interference is expected. This condition is known as the stationary state.

Demanding stationary state, equation 14 reduces to

$$\sin(\alpha)\cos(\alpha - \beta) - 2\sin(\alpha - \beta)\cos(\alpha) = 0$$

which can be rewritten to

$$2\tan(\alpha - \beta) = \tan(\alpha). \tag{15}$$

The trigonometric relation $\tan(\alpha - \beta) = \frac{\tan(\alpha) - \tan(\beta)}{1 + \tan(\alpha)\tan(\beta)}$ can be used to rewrite equation 15 to

$$2\left(\frac{\tan(\alpha) - \tan(\beta)}{1 + \tan(\alpha)\tan(\beta)}\right) = \tan(\alpha).$$

Multiplying both sides by $(1 + \tan(\alpha)\tan(\beta))$ and separating the variables leads to

$$\tan(\beta) = \frac{\tan(\alpha)}{\tan^2(\alpha) + 2} \tag{16}$$

which relates the angle β to the angle α. For this relation the stationary state can again be invoked. So, the observed waves, which are caused by constructive interference, should satisfy $\frac{\partial \beta}{\partial \alpha} = 0$.

The derivative of equation 16 is given by

$$\sec^2(\beta)\frac{\partial \beta}{\partial \alpha} = \frac{(\tan^2(\alpha) + 2)\sec^2(\alpha) - \tan(\alpha)(2\tan(\alpha)\sec^2(\alpha)}{(\tan^2(\alpha) + 2)^2}$$

dividing by $\sec^2(\beta)$ and further simplifying lead to

$$\frac{\partial \beta}{\partial \alpha} = \frac{2 - \tan^2(\alpha)}{(\tan^2(\alpha) + 2)^2}. \tag{17}$$

Demanding that $\frac{\partial \beta}{\partial \alpha} = 0$ combined with equation 17 yields

$$\tan(\alpha) = \pm\sqrt{2},$$

which can be easily solved to find

$$\alpha = \arctan(\pm\sqrt{2}) = \pm\arctan(\sqrt{2}) \approx \pm 54.7^\circ. \tag{18}$$

Finally the Kelvin angle β can be calculated using equation 16

$$\beta = \arctan\left(\frac{\tan(\alpha)}{\tan^2(\alpha) + 2}\right) = \arctan\left(\frac{\pm\sqrt{2}}{4}\right) \approx 19.47^\circ. \tag{19}$$

So, mathematically it was derived that the transverse waves have an angle α of 54.7° and these result in a Kelvin envelope with a half-angle β of 19.47°, leading to a total Kelvin angle of approximately 39°.

B Supplemental Figures

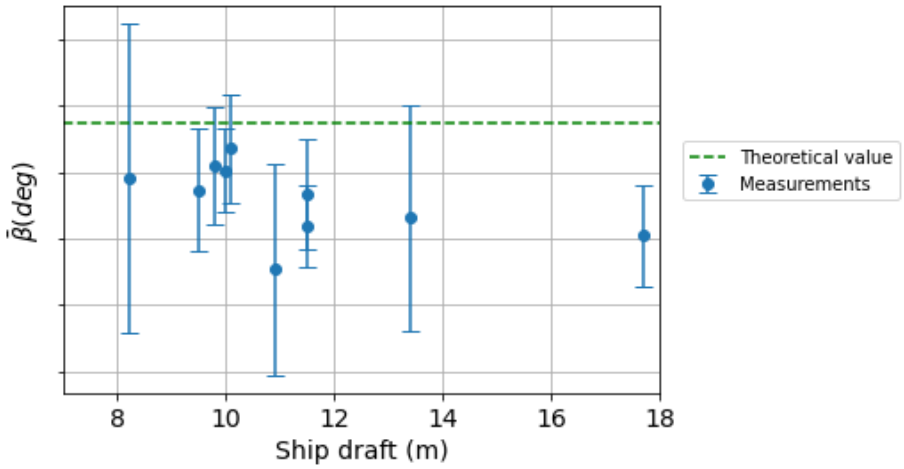

captionMean Kelvin angle $\bar{\beta}$ as a function of the ship draft based on 11 ship images is displayed in blue. The reduction in data points is a result of the dependence on AIS data, which was only coupled successfully in 11 images. The theoretical value for the Kelvin angle of 19.47° is displayed as a dashed green line.

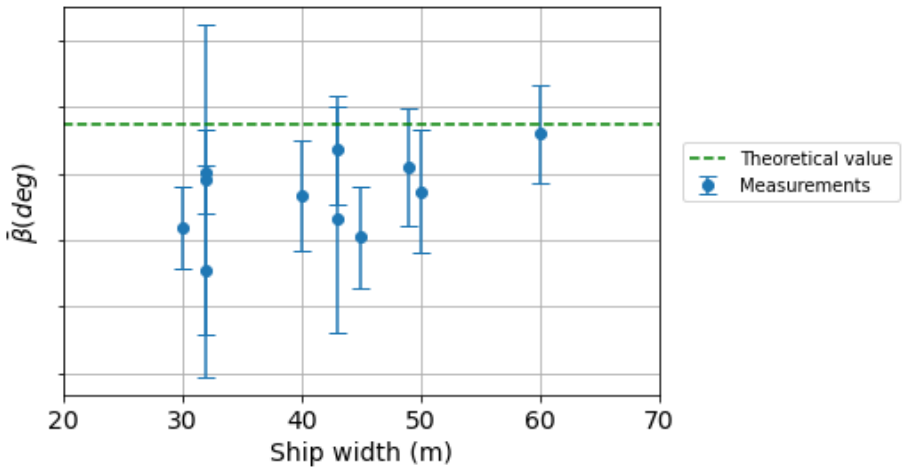

Figure 33: Mean Kelvin angle $\bar{\beta}$ as a function of the ship width based on 11 ship images is displayed in blue. The reduction in data points is a result of the dependence on AIS data, which was only coupled successfully in 11 images. The theoretical value for the Kelvin angle of 19.47° is displayed as a dashed green line.

C Python code

The code used in this project can be found at: `https://github.com/Rubenscheffer/KelvinWakes`